mathematics

MDPI

Article

Computational Investigation of Long Free-Span Submarine Pipelines with Buoyancy Modules Using an Automated Python–Abaqus Framework

Ty Phuor [1], Pavel A. Trapper [2], Alon Urlainis [1,*] and Avshalom Ganz [1]

[1] Department of Civil Engineering, Ariel University, Ariel 40700, Israel; ty168.utp@gmail.com (T.P.); aganz@ariel.ac.il (A.G.)
[2] Department of Civil and Environmental Engineering, Ben-Gurion University of the Negev, Beer-Sheva 84105, Israel; trapper@bgu.ac.il
* Correspondence: alonu@ariel.ac.il

Abstract: This paper introduces an efficient and automated computational framework integrating Python scripting with Abaqus finite element analysis (FEA) to investigate the structural behavior of long free-spanning submarine pipelines equipped with buoyancy modules. A comprehensive parametric study was conducted, involving 1260 free-spanning submarine pipeline models, and was successfully performed with a wide range of parameters, including the length (l_p = 100, 200, and 300 m), radius (r_p = 0.3, 0.4, and 0.5 m), thickness, type of fluid, type of support, load ratio (LR = 0.2, 0.4, 0.6, 0.8, and 1), and number of buoyancy modules (n = 0, 1, 2, 3, 5, 7, and 9) with its length $\left(l_b = 1/10 \cdot l_p\right)$. The study included a verification process, providing a verification of the presented framework. The results demonstrate excellent agreement with analytical and numerical solutions, validating the accuracy and robustness of the proposed framework. The analysis indicates that pipeline deformation and natural frequency are highly sensitive to variations in buoyancy arrangements, pipeline geometry, and load conditions, whereas the normalized mode shapes remain largely unaffected. Practical implications include the ability to rapidly optimize buoyancy module placements, reducing resonance risks from vortex-induced vibrations (VIVs), thus enhancing the preliminary design efficiency and pipeline safety. The developed approach advances existing methods by significantly reducing the computational complexity and enabling extensive parametric analyses, making it a valuable tool for designing stable, cost-effective offshore pipeline systems.

Keywords: long pipeline; free spanning; buoyancy module; submarine pipeline; natural frequency; vortex-induced vibration

MSC: 65

check for updates

Academic Editor: László Péter Kiss

Received: 12 March 2025
Revised: 17 April 2025
Accepted: 22 April 2025
Published: 24 April 2025

Citation: Phuor, T.; Trapper, P.A.; Urlainis, A.; Ganz, A. Computational Investigation of Long Free-Span Submarine Pipelines with Buoyancy Modules Using an Automated Python–Abaqus Framework. *Mathematics* **2025**, *13*, 1387. https://doi.org/10.3390/math13091387

Copyright: © 2025 by the authors. Licensee MDPI, Basel, Switzerland. This article is an open access article distributed under the terms and conditions of the Creative Commons Attribution (CC BY) license (https://creativecommons.org/licenses/by/4.0/).

1. Introduction

Submarine pipelines play a crucial role in offshore oil and gas transportation, extending hundreds of kilometers to connect production sites, processing facilities, and distribution networks. These pipelines are essential for conveying hydrocarbons between offshore infrastructure such as manifolds, wellheads, and platforms, and onshore processing units. Recognized as a cost-effective solution for transporting oil and gas in marine environments [1–3], submarine pipelines are widely used in deep-water and shallow-water developments.

However, budget constraints and challenging seabed conditions—including pipeline crossings, seabed erosion, uneven terrain, and structural tie-ins—often make complete burial impractical [4,5]. As a result, free-spanning pipeline sections are frequently encountered, appearing either as single spans or multiple consecutive spans along the pipeline route.

The design of free-spanning pipelines presents two primary structural challenges: First, vortex-induced vibrations (VIVs) occur when ocean currents interact with the pipeline, generating oscillatory motion. If sustained, these vibrations can lead to fatigue failure over time, as alternating vortex shedding induces cyclic loading on the structure [6–11]. Second, excessive structural stress arises from the combined weight of the pipeline and its internal contents, creating high-stress concentrations that increase the likelihood of localized deformation and potential failure [12–15].

To ensure the safety of free-span pipelines, numerous researchers and practical engineers recommend assessing the actual free span against a maximum allowable free span length [6,12,16]. For instance, DNVGL-RP-F105 [17] suggests remedial actions such as utilizing grout bags, sandbags, and mechanical rigid supports to rectify the free span. However, these measures become extremely expensive and difficult to implement when dealing with deep-water scenarios, such as crossings over underwater valleys at depths of 1500 to 2000 m, and the pressure response in pipelines [18]. Consequently, investigating the stability of free-spanning pipelines has become a crucial study area for the petroleum industry.

VIVs occur in symmetrical or asymmetrical forms, depending on the flow velocity of the ocean currents [5,19]. At low flow velocities, symmetrical vortex shedding generates in-line vibrations, where the oscillations align with the flow direction. At higher flow velocities, asymmetrical vortex shedding induces both in-line and cross-flow vibrations, with the latter occurring perpendicular to the flow direction. Specifically, in-line impulses coincide with each vortex shedding event, while cross-flow impulses act perpendicular to the flow. As a result, the frequency of in-line excitation may be twice that of cross-flow excitation, leading to smaller stress and motion amplitudes in in-line vibrations compared to cross-flow vibrations, where larger oscillations and greater structural stresses are observed [20].

From an engineering perspective, resonance occurs when vortex shedding, defined by the frequency of hydrodynamic forces influenced by the flow velocity, pipe outer diameter, and Strouhal number, aligns with the natural frequency of the free-spanning pipeline [21–25]. When resonance takes place, the pipeline undergoes significant deformations and elevated stress levels, which can ultimately lead to structural failure.

Consequently, extensive research has been conducted to determine the natural frequency of submarine pipelines, as a means to mitigate vibration amplitudes and cyclic stresses. This frequency serves as a key parameter in evaluating pipeline stability [1,5,26]. Ref. [1] proposed an analytical solution based on a linear elastic beam model without axial force to estimate the frequency. Xiao and Zhao [5] extended this approach by incorporating axial forces and boundary conditions, developing a simplified equation to compute the frequency for a 50-m-long pipeline. Their findings indicated that applied tensile forces reduce frequency, while compressive forces increase it. Considering seabed soil characteristics, Yaghoobi et al. [26] introduced an analytical model for offshore pipelines up to 80 m in length, concluding that decreasing soil stiffness leads to a reduction in frequency, significantly influencing pipeline behavior. Additionally, Sarkar and Roy [27] employed the DNVGL-RP-F105 guidelines [17] alongside the finite element method (FEM) to conduct parametric studies. Their analysis, which examined various thicknesses, diameters, span lengths, and homogeneous soil stiffness values, enabled them to estimate the frequency for pipelines up to 100 m in length.

Moreover, Sarkar and Roy [27,28] utilized Abaqus to determine the frequency of pipelines supported by nonhomogeneous soil stiffness. DNVGL-RP-F105 [17], a widely recognized design practice in the oil and gas industry for free-spanning offshore pipelines, was used to develop a closed-form solution that considers the effects of soil stiffness, axial forces, and static deformation in frequency calculations. However, it should be noted that the existing frequency computation solutions are limited to $L/D \leq 140$ [16], where D represents the diameter of the pipe and L denotes the length of the free span. In certain scenarios, such as crossing over canyons or submarine valleys [18], it becomes unavoidable to employ very long free-spanning pipelines. The reports indicate that the gap between the seabed and the pipeline could reach up to 50 m, with free-span pipelines extending up to 500 m [29]. Consequently, rectifying such long free spans can be extremely challenging and costly [17].

To address this challenge, a more practical and cost-effective solution involves the installation of buoyancy modules [4]. However, there is a lack of clear guidance on the optimal configuration of buoyancy modules to achieve design optimization [16]. Recognizing this gap, Trapper [3] conducted a study using a numerical model for geometrically nonlinear analysis to improve the performance of long free-spanning pipelines through the use of buoyancy modules. However, his numerical model was limited to static analysis. Furthermore, for long free-spanning marine pipelines where the ratio of length (L) to diameter (D) exceeds 140, DNVGL-RP-F105 [17] recommends employing finite element analysis (FEA), which is widely recognized as an efficient approach for solving geotechnical [30] and structural engineering problems in such cases [31–33].

Consequently, 3D FEA-based analyses of free-spanning undersea pipelines with buoyancy modules are typically conducted using commercial software such as Abaqus, Riflex, Offpipe, and OrcaFlex [34,35]. However, when performing a large number of simulations, these programs can be computationally intensive and inefficient, as their complex model definitions and data processing workflows depend on cumbersome Graphical User Interfaces (GUIs), making the process time-consuming and impractical for large-scale parametric studies [4,36].

Given these limitations, there is a critical need for a streamlined and automated computational framework that is capable of efficiently handling large datasets while minimizing manual intervention and processing time. An integrated system that enables the automated definition, execution, and extraction of key parameters and essential outputs in a single step would significantly enhance computational efficiency and facilitate preliminary design assessments for offshore pipelines.

Furthermore, despite the growing importance of buoyancy-assisted stabilization, research on the behavior of long free-span pipelines equipped with buoyancy modules remains limited. Addressing this gap requires a robust, scalable, and automated approach that is capable of systematically evaluating the influence of buoyancy configurations on structural performance and VIV mitigation, thereby contributing to the development of more efficient and cost-effective offshore pipeline stabilization strategies.

To achieve these objectives, this paper presents a comprehensive investigation into the behavior of long free-spanning undersea pipelines with buoyancy modules, utilizing an in-house computational framework developed in a Python environment. The proposed framework was designed to compute deformations, extract mode shapes, and determine natural frequencies, incorporating the combined effects of buoyancy through finite element analysis (FEA), using Abaqus as the computational engine.

A large-scale parametric study was conducted, considering a range of pipeline lengths, diameters, and thicknesses, along with various buoyancy configurations and load ratios. These simulations enabled a detailed assessment of buoyancy modules' effectiveness in mit-

igating vortex-induced vibrations (VIVs). Furthermore, the accuracy of the framework was validated by comparing the computed deformations and natural frequencies of free-spanning submarine pipelines against existing analytical and numerical solutions, demonstrating strong agreement and confirming the reliability of the proposed methodology.

2. Materials and Methods

2.1. Abaqus-Based Computational Framework

This study introduces a Python–Abaqus integrated computational framework for performing large-scale numerical simulations of long free-span submarine pipelines with buoyancy modules, as depicted in Figure 1. The proposed framework leverages Abaqus [37] finite element analysis (FEA) as the computational solver, while custom-developed Python scripts automate the key processes of model setup, simulation execution, and post-processing of results. A diagram illustrating the key Python classes and methods involved in the framework's preprocessing, model generation, and post-processing stages is provided in Appendix A.

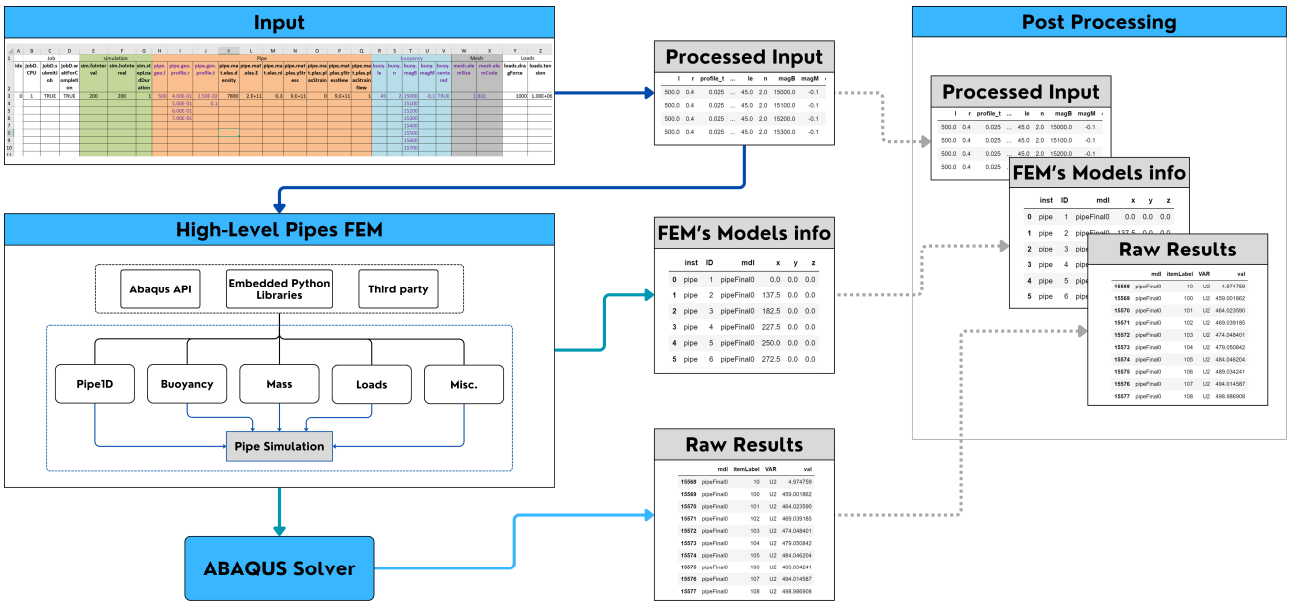


Figure 1. Schematic representation of the Abaqus-based computational framework.

The simulation workflow comprises six main stages (Figure 2):

2.1.1. Step 1: Input Data Preparation

Initially, the simulation parameters are organized systematically into an Excel (version 2023, Microsoft Corporation, Redmond, WA, USA) input file. A dedicated Python (version 2.7, Python Software Foundation, Wilmington, DE, USA) preprocessing script then reads and processes these parameters, creating distinct numerical pipeline models. Each row within the Excel sheet represents a unique pipeline configuration, including geometry and material properties. The preprocessing stage generates a binary dictionary file (pMI) containing model-specific parameters, as well as a structured Pandas DataFrame file (pMIp) that ensures organized and efficient data handling for subsequent analysis.

2.1.2. Step 2: Model Generation and Execution

Following data preparation, a dedicated Python (version 2.7, Python Software Foundation, Wilmington, DE, USA) script automatically processes the structured input, generating the finite element models required for analysis. This Python script produces several key

files, including a CAE file containing comprehensive model details for use within Abaqus (version 2023, Dassault Systèmes, Vélizy-Villacoublay, France), a geometry definition file (pM file), and an output database (ODB file) that stores the numerical results from the Abaqus simulations. The automation of this step ensures consistency across simulations and significantly reduces manual input effort.

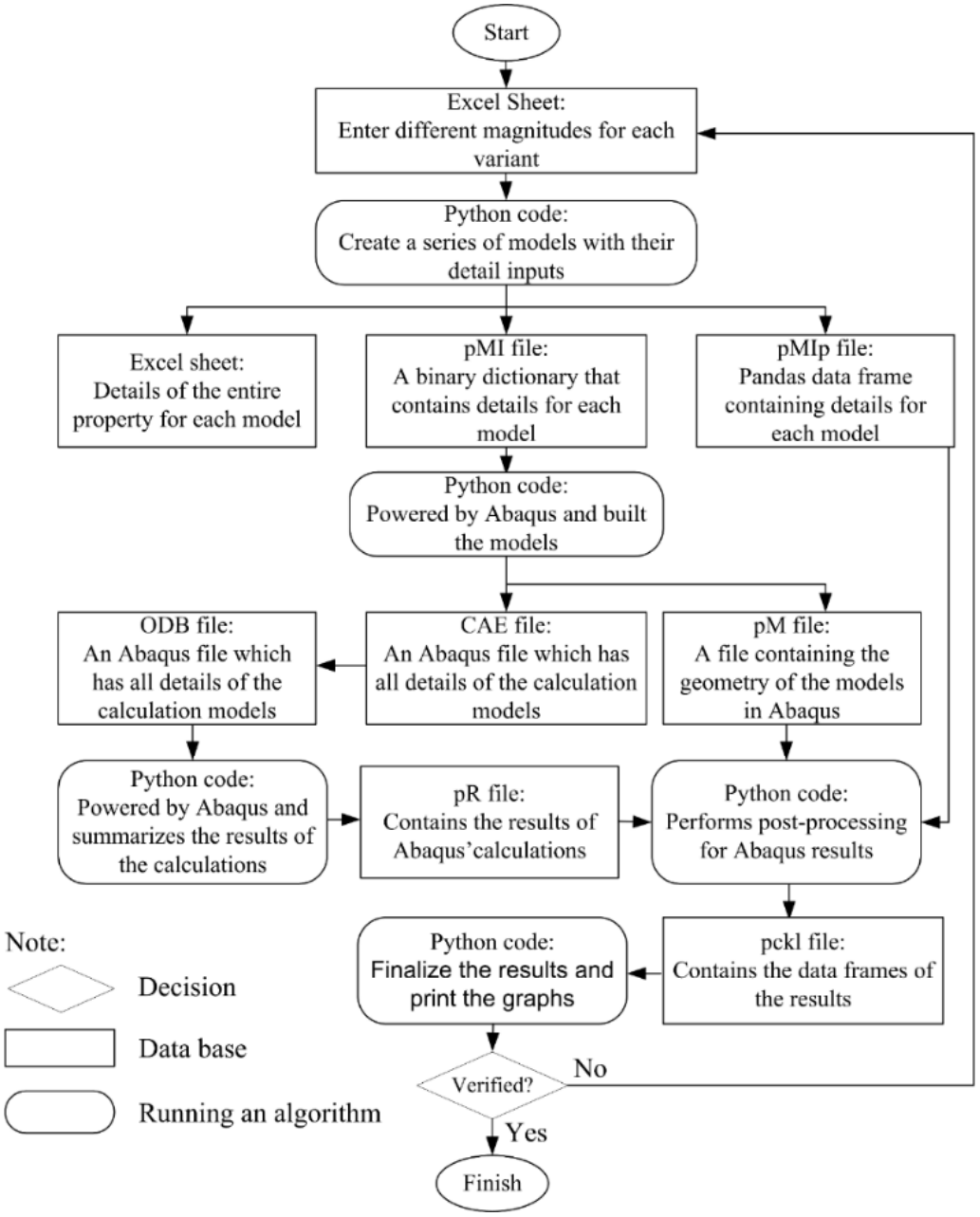


Figure 2. Flowchart illustrating the detailed workflow of the proposed Python–Abaqus computational framework.

2.1.3. Step 3: Extraction of Computational Results

Upon completion of the simulations, another Python (version 3.9, Python Software Foundation, Wilmington, DE, USA) script systematically extracts the critical computational outcomes from the Abaqus-generated ODB files, creating a result summary file (pR file). This file contains essential pipeline response parameters, such as deformation, stress distributions, and natural frequencies, facilitating efficient access and preliminary analysis of simulation results.

2.1.4. Step 4: Data Structuring for Comprehensive Analysis

Next, a dedicated Python (version 3.9, Python Software Foundation, Wilmington, DE, USA) script consolidates the previously obtained data into a single structured file (pckl file). This integrated file merges the simulation parameters and corresponding results, allowing for seamless and efficient analysis of deformation and frequency response across multiple pipeline configurations.

2.1.5. Step 5: Evaluation and Visualization of Results

Using the consolidated structured data, the Python (version 3.9, Python Software Foundation, Wilmington, DE, USA) environment enables the visualization and analysis of the results. This step includes generating curves for deformation and natural frequency as a function of key pipeline parameters, such as the length-to-diameter ratio (L/D). These graphical representations facilitate a detailed understanding of pipeline performance and help identify optimal buoyancy module configurations.

2.1.6. Step 6: Verification, Refinement, and Convergence

Finally, the accuracy and reliability of the simulation results are carefully verified. If discrepancies or inconsistencies are detected, adjustments to the input parameters are made, and the simulation process is repeated from Step 1. This iterative verification cycle continues until the simulations converge satisfactorily, ensuring robust and reliable outcomes that are suitable for practical engineering design decisions.

This automated approach drastically reduces the time required for conducting parametric studies, while ensuring consistency and repeatability in large-scale simulations.

2.2. Computation of Effective Density and Force Vectors with Buoyancy Modules

In the context of long free-spanning submarine pipelines, accurately determining the natural frequency is crucial for assessing pipelines' vulnerability to vortex-induced vibrations (VIVs). In the proposed computational framework, the free-spanning pipeline equipped with buoyancy modules is represented using a two-node beam element featuring 12 degrees of freedom (DOF). Rather than explicitly modeling buoyancy modules geometrically, their effects are represented indirectly through the assignment of different effective densities to pipeline sections with and without buoyancy. This approach is necessary for facilitating accurate modal and structural analyses within the Abaqus-based computational framework.

Consequently, the framework employs different effective masses for the pipe and buoyancy sections, expressed as Equations (1) and (2), respectively, to facilitate the computation of the natural frequency.

$$m_{e,fpc} = m_p + m_c + m_f + m_{w,fpc} \qquad \text{(pipe section)} \tag{1}$$

$$m_{e,b} = m_p + m_c + m_f + m_{w,b} \qquad \text{(buoyancy module section)} \tag{2}$$

where m_p, m_c, m_f, $m_{w,fpc}$, and $m_{w,b}$ are the mass of the steel pipe; the mass of the coating; the mass of the fluid (oil, gas, etc.); the mass of pushed water displaced by the fluid, pipe, and concrete; and the mass of pushed water displaced by the fluid, pipe, concrete, and buoyancy module, respectively. Subsequently, the force vectors to the correct static deformation can be computed as shown in Equations (3) and (4):

$$F_{pipe} = 2 \times A_{fpc} \times \rho_w \times g \qquad \text{(pipe section)} \tag{3}$$

$$F_{buoyancy} = 2 \times A_{bNp} \times \rho_w \times g \qquad \text{(buoyancy module section)} \tag{4}$$

where g, A_{fpc}, A_{bNp}, and ρ_w are the gravitational acceleration; the cross-sectional area of the fluid, pipe, and coating; the cross-sectional area of the buoyancy module; and the density of seawater. It is important to highlight that the cross-sectional area of the buoyancy module (A_b) can be determined based on the provided load ratio, which represents the ratio of the total lifting weight of the buoyancy module to the combined weight of the fluid, pipe, and coating. This load ratio serves as a guide for calculating the appropriate size of the buoyancy module's cross-section.

2.3. Verification

To ensure the reliability and accuracy of the developed Python–Abaqus computational framework, a comprehensive verification procedure was conducted. In this study, the model results were validated against analytical solutions from the previous literature, as well as finite element results obtained using Abaqus. The verification focused on computing the static deformations and natural frequencies of long submarine pipelines without buoyancy. The lengths chosen for verification included 10, 15, 20, 25, 35, 45, 50, 100, 200, 400, 600, and 800 m. Furthermore, when the buoyancy module was incorporated into the pipeline, the hand calculations for the effective masses (or densities) and vertical forces in the Abaqus-based framework were also verified. The pipeline properties, along with other parameters, are detailed in Table 1.

Table 1. Material and geometric properties used for pipeline model verification.

Input Data	Value
Pipe's thickness (t_p)	0.015 m
Pipe's radius (r)	0.35 m
Density of steel pipe	7850 kg/m^3
Pipe's Young's modulus (E)	206 GPa
Pipe's Poisson ratio	0.30
Coating's construction strength	30.00 MPa
Coating's thickness	0.01 m
Density of coating	3040 kg/m^3
Density of seawater	1025 kg/m^3
Density of the fluid inside the pipe	442 kg/m^3

The material and geometric properties summarized in Table 1 are representative values that were selected to ensure consistency and facilitate comparative analyses across the parametric simulations. While representative, these values remain within realistic ranges typical in submarine pipeline design and analysis, as documented by guidelines [1,17]. The pipe dimensions and material properties correspond to typical carbon steel specifications, and a 10 mm concrete coating was applied in the simulations. The seawater density reflects typical marine conditions, and the internal fluid density specifically represents compressed natural gas. Verification analyses were conducted using fixed–fixed (FF) and pinned–pinned (PP) support configurations to comprehensively assess the computational framework's robustness.

It should be noted that experimental validation was not performed due to practical limitations, including high costs, logistical complexities, regulatory coordination, and limited site access associated with full-scale tests on long free-spanning submarine pipelines under variable buoyancy conditions. Nevertheless, validation against established theoretical and numerical studies ensured the robustness and accuracy of the presented model.

2.3.1. Verification of the Computed Frequency and Deformation of Pipelines Without Buoyancy Modules

The verification process began by computing the natural frequencies of pipelines measuring 15, 25, 35, and 45 m in length, each with a diameter of 0.254 m and a thickness of 0.011 m. The corresponding material properties, as outlined in Table 1, were employed. Figure 3 presents a comparison of the computed natural frequencies obtained via the proposed framework with both analytical and numerical reference solutions, for pipelines with and without internal fluid under fixed–fixed (FF) and pinned–pinned (PP) boundary conditions. The strong agreement observed across all cases corroborates the accuracy and robustness of the proposed computational model.

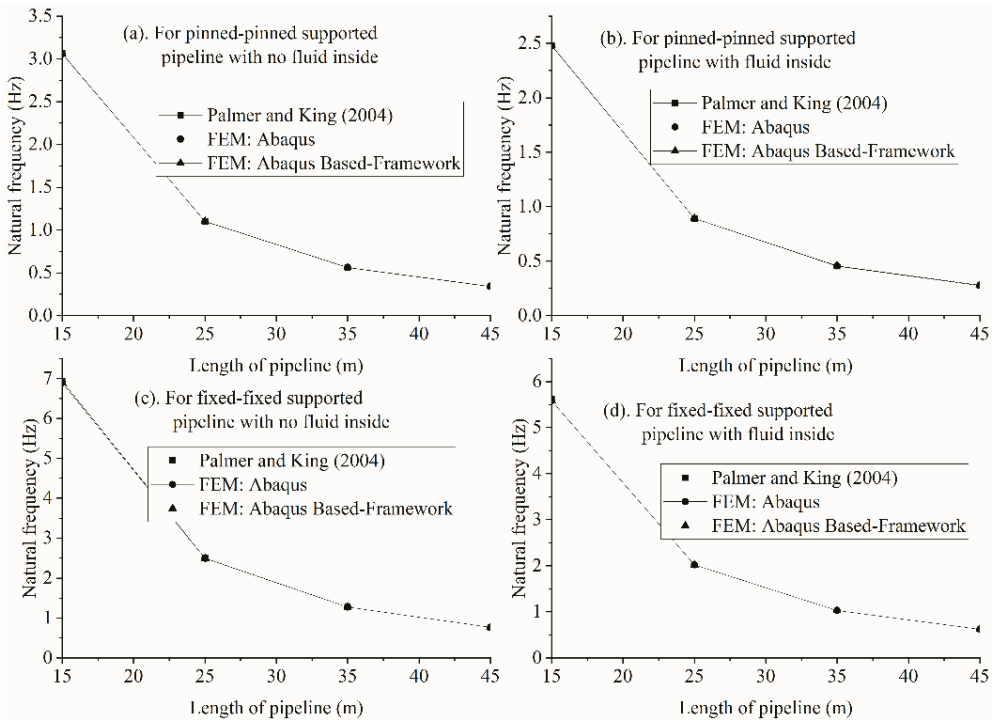


Figure 3. Comparison of natural frequencies computed by the present method with the existing available solutions produced by Palmer and King [1] and Abaqus [37].

Further verification analyses were performed by conducting additional pipeline simulations using the material and geometric properties detailed in Table 1. Figure 4 provides a comparison of the fundamental natural frequency (Freq) and static deformation (Def) of the free-spanning submarine pipeline (D = 0.7 m). The calculations were performed using the developed framework (PS), Abaqus, and an analytical method for various combinations of the thickness (with D/t ratios of 10, 20, and 40) and length (L = 10, 20, 50, 100, 200, 400, 600, and 800 m) of a pipe with fixed–fixed support.

It can be seen that the current solutions are in excellent agreement with those calculated by Abaqus [38] for all cases. In addition, the results indicate that the computed solutions for lengthy pipelines show reasonable agreement with the analytical solutions obtained by Phuor et al. [16]. Particularly, for $L \geq 100$ m, the two methods exhibit a satisfactory level of agreement. However, notable discrepancies arise when $L < 100$ m. For L = 100 m and L = 800 m, relative errors of 0.61%, 1.5%, 12% and 23%, 26%, 36% were recorded for D/t ratios of 10, 20, and 40, respectively. Furthermore, it was observed that the deformations calculated by both methods gradually decreased as the thickness and length of the pipe decreased.

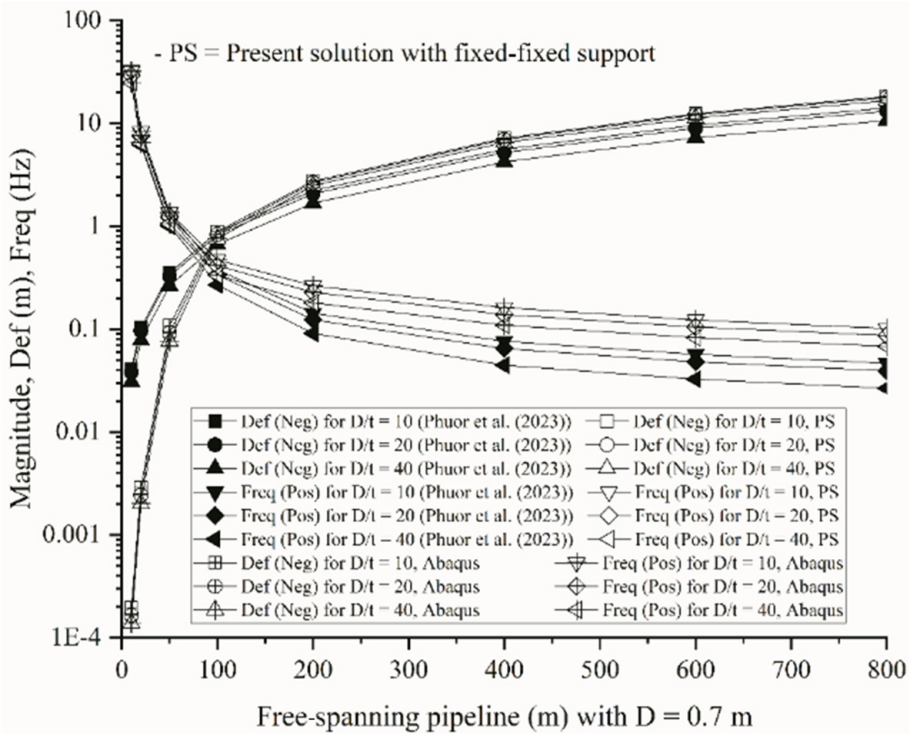


Figure 4. Comparison of static deformation (Def) and fundamental natural frequency (Freq) for a fixed–fixed free-spanning pipeline (D = 0.7 m) at various span lengths (up to 800 m) and different diameter-to-thickness ratios (D/t = 10, 20, 40). Results from the present solution (PS) are plotted alongside those obtained by Phuor et al. (2023) [16] and Abaqus [38].

Furthermore, additional verification simulations were conducted, as presented in Figure 4, which shows that the fundamental natural frequency gradually increases as the pipeline length decreases and the pipe thickness increases. Specifically, the relative errors for diameter-to-thickness (D/t) ratios of 10, 20, and 40 were found to be 0.9%, 2.7%, and 4.2%, respectively, reflecting close agreement with the analytical solutions. The relative errors increased with higher D/t ratios and longer pipeline lengths, reaching up to 12% for pipelines with an 800 m span. Overall, these observations highlight that the relative errors in computed frequencies decrease with shorter pipeline lengths and lower D/t ratios, confirming that the computational framework provides satisfactory accuracy for pipelines with fixed–fixed boundary conditions.

Figure 5 provides a comparison for a pinned–pinned free-spanning pipeline. The magnitudes of the deformations decrease as the length and thickness of the pipelines decrease. Additionally, the natural frequency values decrease as the length of the pipeline increases and the thickness decreases. These observations highlight the relationship between deformations, natural frequency, and the varying dimensions of the pipeline. Furthermore, Figure 5 demonstrates that the deformations and frequencies computed by the proposed framework closely match those obtained from Abaqus and show reasonable agreement with the analytical solution obtained by Phuor et al. [16] for pipeline lengths of at least 100 m. However, a notable discrepancy can be observed for pipeline lengths below 100 m. It is important to highlight that analyzing the free-spanning pipeline using the developed framework becomes challenging for small-diameter pipes with large thicknesses, due to their excessive self-weight. Moreover, it can be observed that the frequency remains nearly constant for a given D/t ratio and as the pipe diameter increases. Additionally, the deformation for the fixed–fixed support configuration is significantly higher than that

for the pinned–pinned support. Conversely, there is virtually no difference in frequency magnitude between the pinned–pinned and fixed–fixed supports.

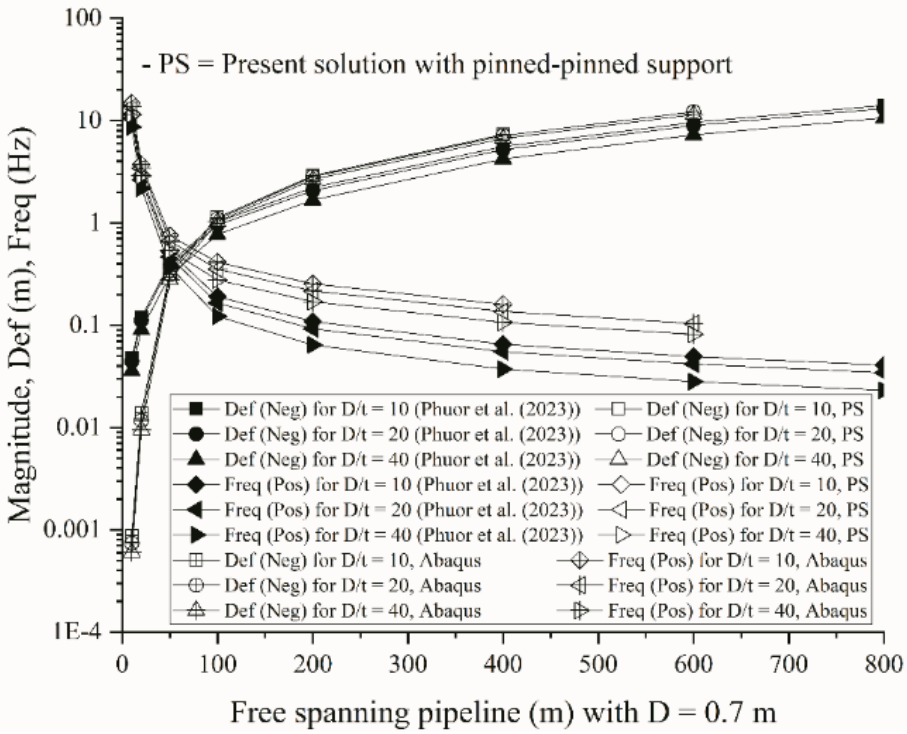


Figure 5. Comparison of static deformation (Def) and fundamental natural frequency (Freq) for a pinned–pinned free-spanning pipeline (D = 0.7 m) at various span lengths (up to 800 m) and different diameter-to-thickness ratios (D/t = 10, 20, 40). Results from the present solution (PS) are plotted alongside those obtained by Phuor et al. (2023) [16] and Abaqus [38].

2.3.2. Verification of the Computed Effective Mass (Density) and Vertical Force Applied to Sections of the Pipeline and Buoyancy Modules

Pipeline Section

Utilizing the parameters presented in Table 1, the effective masses of the pipe, internal fluid, and coating, along with their displaced water components, were calculated for the pipeline section.

$$\rho_{e,fpc} = \frac{m_{e,fpc}}{A_p} = \frac{(m_p + m_c + m_f + m_{w,fpc})}{A_p} = 27,713 \ \frac{\text{kg}}{\text{m}^3}$$

The vertical force required for accurately calculating the static deformation of the pipeline section was determined.

$$F_{pipe} = 2 \times A_{fpc} \times \rho_w \times g = 8188 \ \frac{\text{kN}}{\text{m}}$$

Consequently, the total weight of the fluid, pipe, and coating was computed as follows:

$$W_{fpc,Total} = (\rho_p A_p + \rho_c A_c + \rho_f A_f) \times g \times l_p = 468,190 \text{ kN}$$

Buoyancy Module Section

To calculate the effective density of the buoyancy section, the load ratio (LR) must first be specified. In this verification example, an LR value of 10^{-3} was chosen. Given this load

ratio, the buoyancy module radius (r_b) corresponding to a buoyancy module length of 10 m (one-tenth of the total pipeline length) was computed as follows:

$$W_b = LR \times W_{fpc,Total}$$

$$A_b \times \rho_w \times l_b = LR \times W_{fpc,Total}$$

$$r_b = \sqrt[2]{LR \times \frac{W_{fpc,Total}}{(\pi \times (\rho_w \times l_b))} + (r_{fpc})^2} = 0.35211 \text{ m}$$

The effective mass and, thus, the effective density for the buoyancy module section were calculated as follows:

$$m_{e,b} = m_p + m_c + m_f + m_{w,b}$$

$$\rho_{e,b} = \frac{m_{e,b}}{A_p} = \frac{(m_p + m_c + m_f + m_{w,b})}{A_p} = 27,153 \ \frac{\text{kg}}{\text{m}^3}$$

Subsequently, the vertical force applied to the buoyancy section was determined:

$$F_{buoyancy} = 2 \times A_{bNp} \times \rho_w \times g = 93.63 \ \frac{\text{kN}}{\text{m}}$$

Thus, the total lifting weight provided by the buoyancy modules in static analysis was calculated by

$$W_{buoyancy,Total} = \frac{F_{buoyancy}}{2} \times l_b \times number_{of_{buoyancy}} = 468 \text{ kN}$$

Verifying the load ratio yields

$$LR = \frac{W_{buoyancy,Total}}{W_{fpc,Total}} = 0.000999 \approx 0.001 \leftarrow Verified!$$

This demonstrates close agreement with the intended load ratio, with the minor discrepancy arising due to floating-point arithmetic precision in Python computations. Repeating the procedure for a pipeline length of 100 m with five buoyancy modules, each covering one-tenth of the total pipeline length (maintaining the LR at 0.001), results in effective densities and vertical forces computed as follows: $\rho_{e,fpc} = 27,713 \ \frac{\text{kg}}{\text{m}^3}$, $F_{pipe} = 8188 \ \frac{\text{kN}}{\text{m}}$, $\rho_{e,b,5b} = 27,035 \ \frac{\text{kg}}{\text{m}^3}$, and $F_{buoyancy,5b} = 18.72 \ \frac{\text{kN}}{\text{m}}$.

The verification results confirm that the computations are reliable, demonstrating that increasing the number of buoyancy modules leads to a corresponding decrease in both effective density and vertical force applied to the buoyancy sections, while the computed parameters for the pipeline sections remain consistent.

3. Simulation Results

A series of parametric studies involving multiple free-span underwater pipelines with buoyancy modules were conducted in a range of pipeline lengths of 100, 200, and 300 m. The number of buoyancy modules employed ranged from 1 to 9, with an increment of one, where each buoyancy module's length was equal to one-tenth of the free-spanning pipeline length. To provide visual examples of the buoyancy module arrangements, Figure 6 illustrates three typical configurations: (a) one buoyancy module ($n = 1$), (b) two buoyancy modules ($n = 2$), and (c) three buoyancy modules ($n = 3$). For cases where $n > 3$, the buoyancy modules can be positioned accordingly, following the provided patterns.

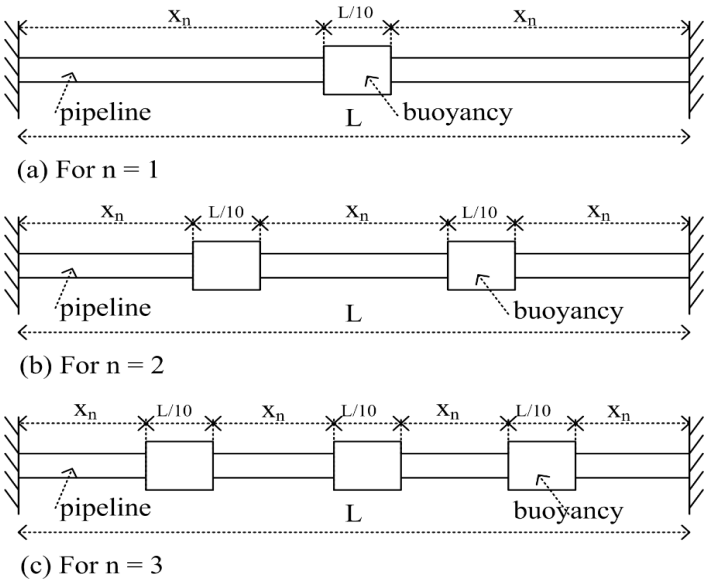


Figure 6. A typical arrangement of the buoyancy modules (the length of each buoyancy module equals a one-tenth of the total length of the pipeline) attached to the underwater pipeline with fixed–fixed supports: (**a**) for one buoyancy module, (**b**) for two buoyancy modules, and (**c**) for three buoyancy modules.

The pipeline input data utilized in this section remain identical to the data employed in Section 3 (Verification). Negligible densities are assigned to both the buoyancy module and its foam. However, if the density of the buoyancy module equals the density of water (i.e., 1025 kg/m^3), it becomes the added mass simulation shown in Figure 7. To ensure a conservative approach, the flexural rigidity of the model is assumed to be the same as that of the steel pipe. The radius of the buoyancy is determined to satisfy the condition where the total weight ($W_{fpc,\ Total}$) of the pipeline model equals the load ratio multiplied by the buoyancy-based uplifted weight ($W_{buoyancy,\ Total}$). In this study, a range of different buoyancy radii were explored, maintaining the relationship $W_{buoyancy,\ Total} = LR \cdot W_{fpc,\ Total}$, where LR varies from 0 to 1 with an increment of 0.2. This allowed for comprehensive parametric investigations to be conducted.

3.1. Investigation of Deformation Analysis of the Free-Span Submarine Pipeline

Figure 7 presents a comparison of the vertical deformation of the pipelines ($r_p = 0.3$ m and thickness $(t_p) = 0.02$ m) with various numbers of buoyancy modules attached ($l_b = 1/10 \cdot l_p$), with different load ratios (i.e., LR = 0.2, 0.4, 0.6, 0.8, and 1, with different colors), against the pipe length resting on the fixed–fixed support. The columns represent different pipe lengths (i.e., 100, 200, and 300 m), and the rows are the number of buoyancy modules ($l_b = 1/10 \cdot l_p$) (i.e., n (=buoyByMode) = 0, 1, 2, 3, 5, 7, and 9). It can be observed that the maximum negative deformation is always found for the pipeline without buoyancy. For pipelines with buoyancy modules, the optimal deformation varies and is strongly dependent on the combination of the number of buoyancy modules and the load ratio. Obviously, to reduce the absolute deformation value of the pipe, it is not necessary to apply a high load ratio with many buoyancy modules. For instance, interestingly, the minimum absolute deformations are found at the combinations of LR = 0.4 and n (=buoyByMode) = 7. It should also be noted that for the added mass simulation, its deformation is equivalent to the deformation of the pipeline without a buoyancy module, because they are both in the same case, where the pipeline is surrounded by water.

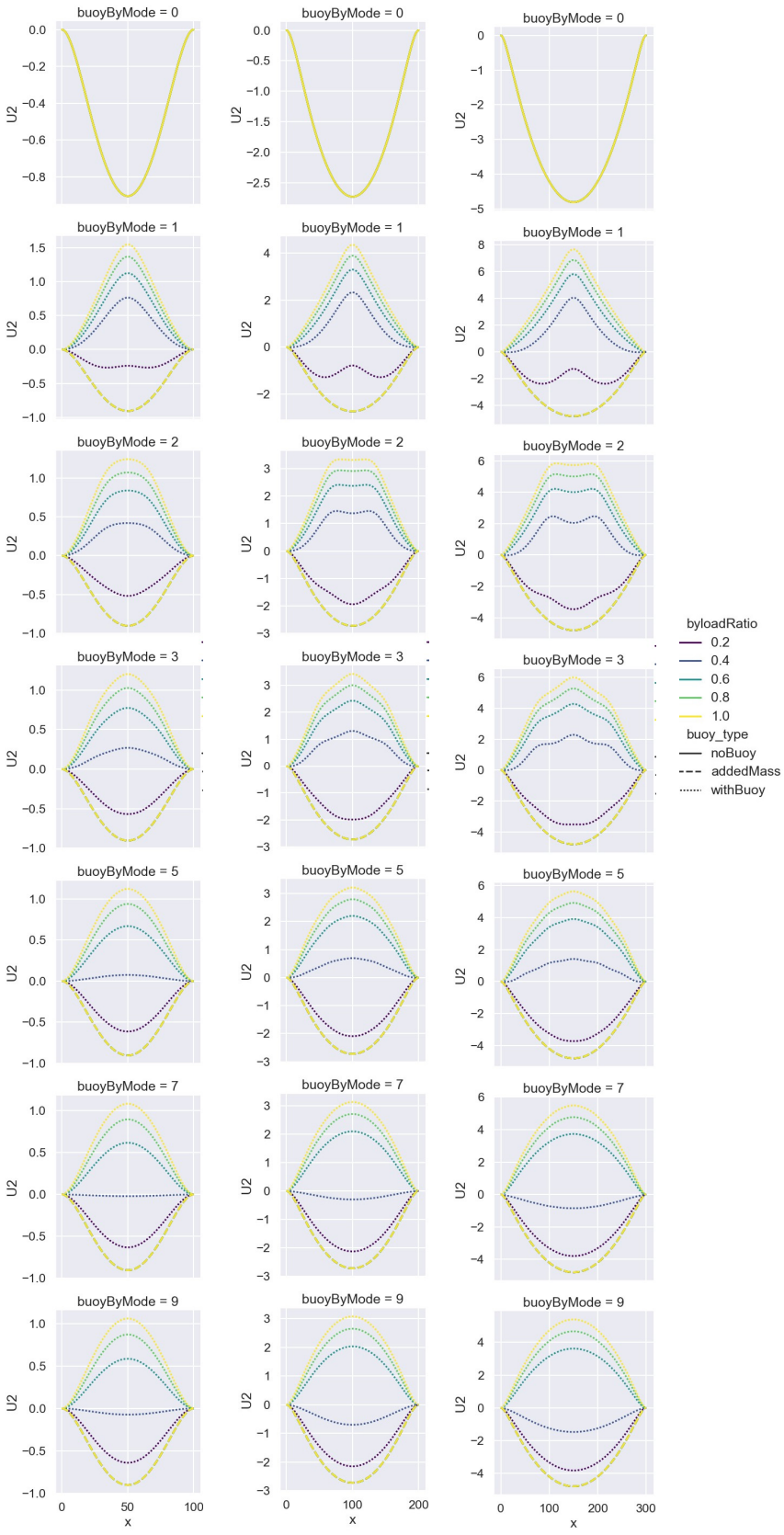


Figure 7. Comparisons of the vertical deformation of the pipelines (r_p = 0.3 m and thickness (t_p) = 0.02 m) with various numbers of buoyancy modules attached ($l_b = 1/10{\cdot}l_p$), with different load ratios (i.e., *LR* = 0.2, 0.4, 0.6, 0.8, and 1, with different colors), against the pipe length resting on the fixed–fixed support, where columns are the pipe length (i.e., 100, 200, 300 m) and rows are the number of buoyancy modules ($l_b = 1/10{\cdot}l_p$) (i.e., n (=buoyByMode) = 0, 1, 2, 3, 5, 7 and 9).

Moreover, when increasing the pipe thickness to 0.03 m, the minimum absolute deformations are found at n = 3 and LR = 0.4 for all pipeline lengths, as shown in Figure 8. On the other hand, when increasing the pipe radius to 0.5 m, as shown in Figure 9, it can be observed that the minimum absolute deformation of all pipeline lengths is found at n = 1 and LR = 0.2.

Similarly, if the radius equals 0.4 m and the thickness equals 0.02 m, the lowest deformations are also found with n = 1 and LR = 0.2, as illustrated in Figure S1 in the Supplementary Materials. However, when the pipe radius and thickness increase to 0.5 m and 0.03 m (see Figure S2), respectively, the lowest minimum deformations are found at n = 9 and LR = 0.4. Consequently, the absolute minimum deformation varies and is strongly dependent on the combination of the number of buoyancy modules, the load ratio, and the pipeline's thickness and radius.

3.2. Investigation of the Analysis of the Natural Frequency of the Free-Span Submarine Pipeline

From an engineering perspective, the natural frequency of a structure typically increases with increasing deformation. The frequency ratio (freqRatio) is computed by dividing the magnitude of the natural frequency of the pipeline with the buoyancy module by the frequency of the pipeline without the buoyancy module. The types of buoyancy module can include those with air and with seawater (also called added mass). The position in which the buoyancy modules are placed is similar to the position of the mode shape of the pipeline; for example, one buoyancy module (freqs_byMode_1) is placed at the middle of the pipeline, corresponding to the intersection point between the pipeline and its second mode shape (in both vertical and horizontal plans).

Figure 10 illustrates the comparisons of the ratio of the natural frequency of the pipelines (length = 100 m, r_p = 0.3 m, thickness = 0.02 m) against the mode numbers (mpN) for various combinations of the buoyancy modules (i.e., n = 1, 2, and 3) and load ratios (i.e., LR = 0.2, 0.4, 0.6, 0.8, and 1), where the columns are the mode plans (i.e., horizontal (left) and vertical (right)) and the rows are the number of buoyancy modules (i.e., 1, 2, and 3 buoyancy modules). From this figure, it can be observed that the magnitudes of the frequency of each mode are slightly different for the vertical and horizontal plans. Additionally, it should also be noted that, for all load ratios (i.e., 0.2, 0.4, 0.6, 0.8, and 1), the maximum frequency ratios are found at the mode plan numbers (mpN) 2, 3, and 4 for 1, 2, and 3 buoyancy modules, respectively. Additionally, similar observations were also made for pipeline lengths of 200 m and 300 m, as depicted in Figures 11 and 12, respectively.

These findings remain consistent when the pipe thickness is raised to 0.03 m (Figure S3) or the pipe radius is increased to 0.5 m (Figure S4). It is generally acknowledged that resonance may occur not only at the fundamental mode but also at higher modes. Consequently, it is worth mentioning that in this study, the collapse of pipelines with and without buoyancy modules due to resonant phenomena at any specific modes might be avoided by reducing the frequency magnitude, by placing the buoyancy module at a location corresponding to that collapsed mode.

3.3. Parametric Analysis of Buoyancy Configurations and Load Ratios

To visualize the effects of different buoyancy configurations and load ratios on the structural performance of free-spanning submarine pipelines, a series of heatmaps were generated. These maps present the computed displacement, von Mises stress, and bending moment across a parametric range of load ratios (0.2 to 1.0) and numbers of buoyancy modules (1 to 9). The analysis is presented for two support conditions—pinned–pinned (Figure 13) and fixed–fixed (Figure 14)—and for two pipe radii: 0.30 m and 0.40 m.

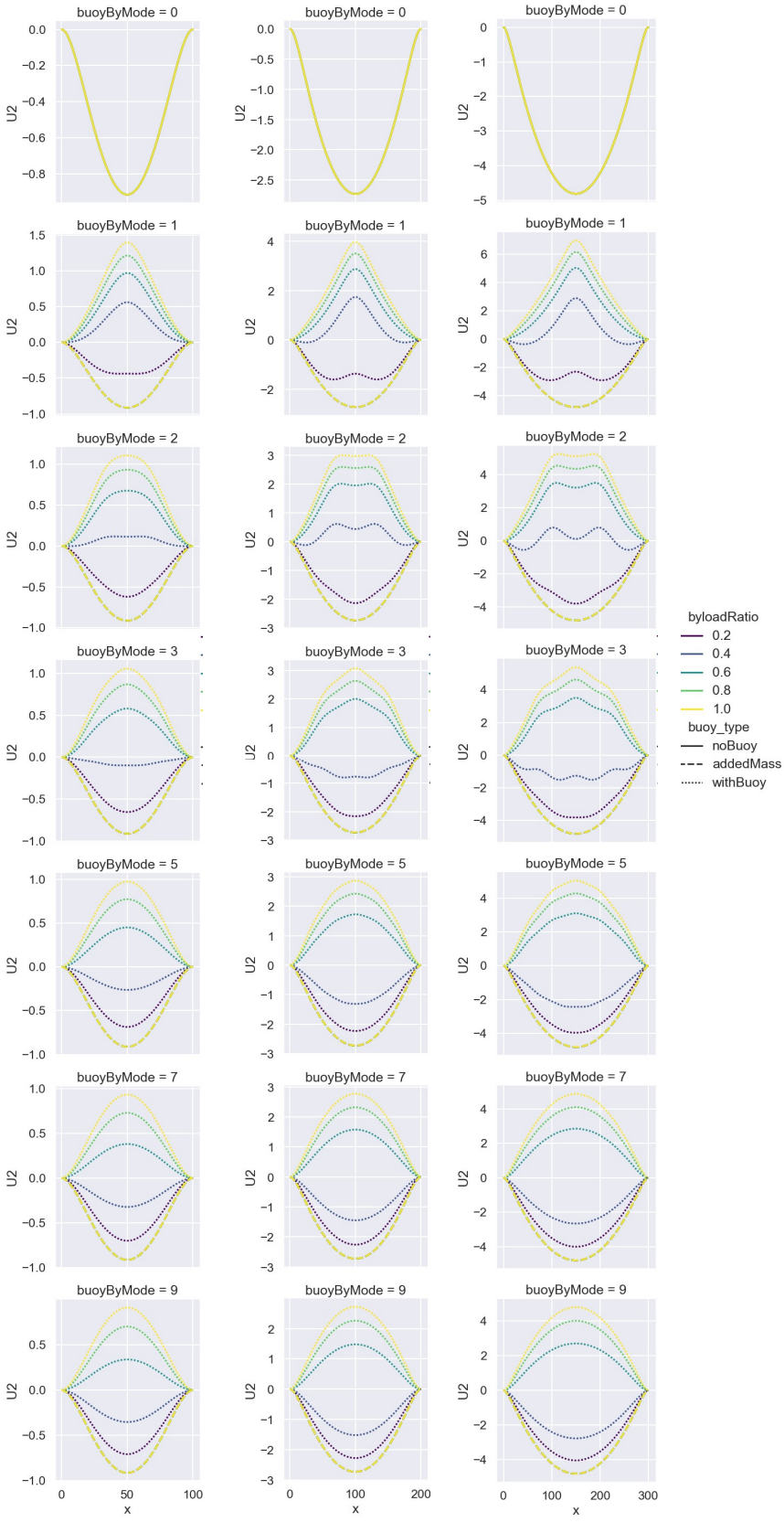


Figure 8. Comparisons of the vertical deformation of the pipelines (r_p = 0.3 m and thickness (t_p) = 0.03 m) with various numbers of buoyancy modules attached ($l_b = 1/10{\cdot}l_p$), with different load ratios (i.e., LR = 0.2, 0.4, 0.6, 0.8, and 1, with different colors), against the pipe length resting on the fixed–fixed support, where columns are the pipe length (i.e., 100, 200, 300 m) and rows are the number of buoyancy modules ($l_b = 1/10{\cdot}l_p$) (i.e., n (=buoyByMode) = 0, 1, 2, 3, 5, 7 and 9).

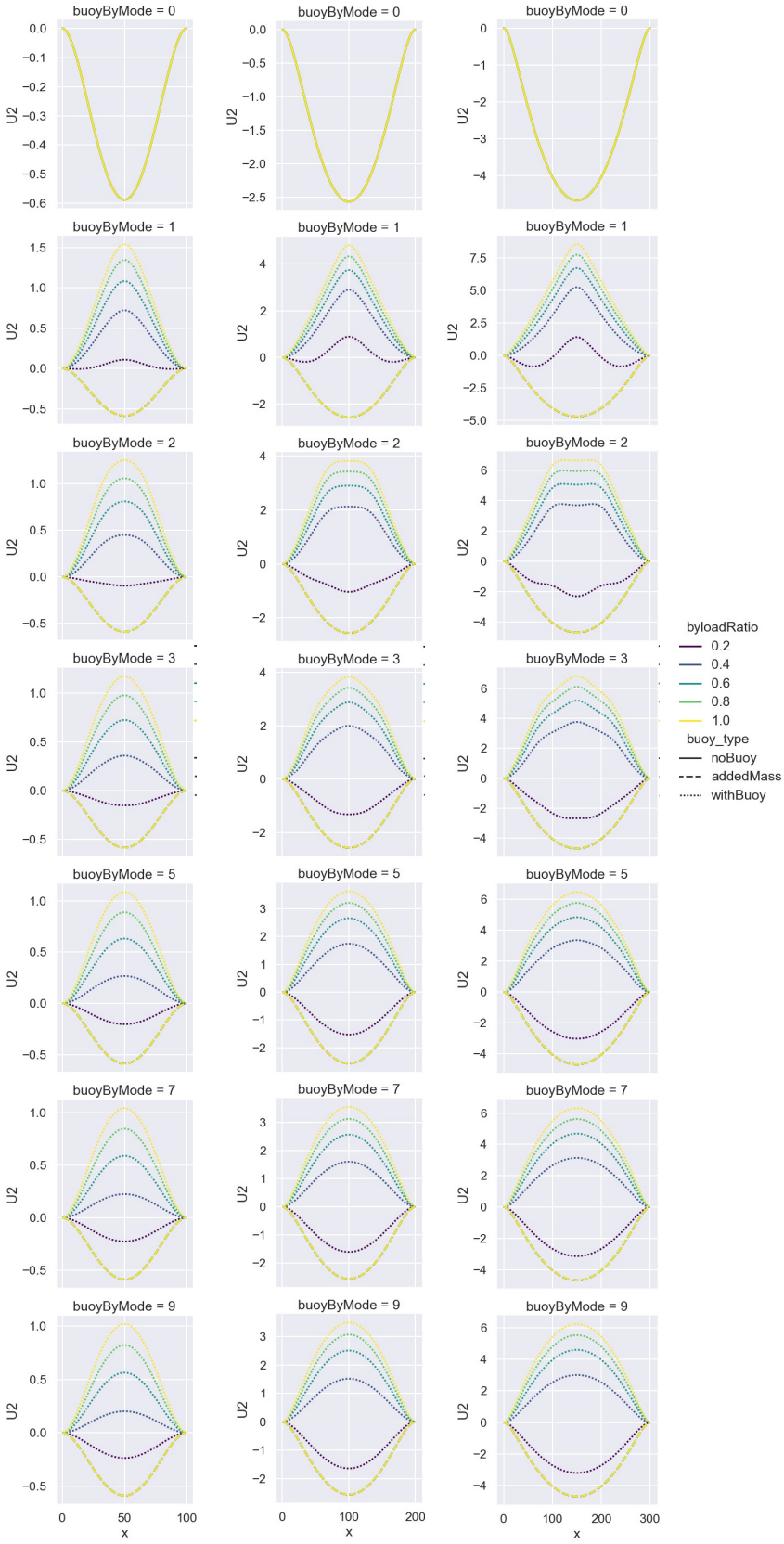


Figure 9. Comparisons of the vertical deformation of the pipelines ($r_p = 0.5$ m and thickness (t_p) = 0.02 m) with various numbers of buoyancy modules attached ($l_b = 1/10{\cdot}l_p$), with different load ratios (i.e., *LR* = 0.2, 0.4, 0.6, 0.8, and 1, with different colors), against the pipe length resting on the fixed–fixed support, where columns are the pipe length (i.e., 100, 200, 300 m) and rows are the number of buoyancy modules ($l_b = 1/10{\cdot}l_p$) (i.e., n (=buoyByMode) = 0, 1, 2, 3, 5, 7 and 9).

Figure 13 presents the parametric results for pinned–pinned pipelines with radii of 0.30 m (a) and 0.40 m (b). For both geometries, the displacement and internal forces generally increase with higher load ratios and decrease with an increasing number of buoyancy modules. However, this relationship is not strictly monotonic, indicating that optimal configurations do not necessarily involve the highest number of modules. Specifically, the U2_heatmap shows that the lowest displacement values occur at a load ratio of 0.4, with buoyancy module counts (buoyByMode) of 5 and 7. The MISES_heatmap, which presents von Mises stress values, also reflects a similar trend. Stress magnitudes increase with the load ratio due to greater uplift forces, but the lowest stress values are found at a load ratio of 0.4 and buoyByMode values of 5 and 7, mirroring the displacement results.

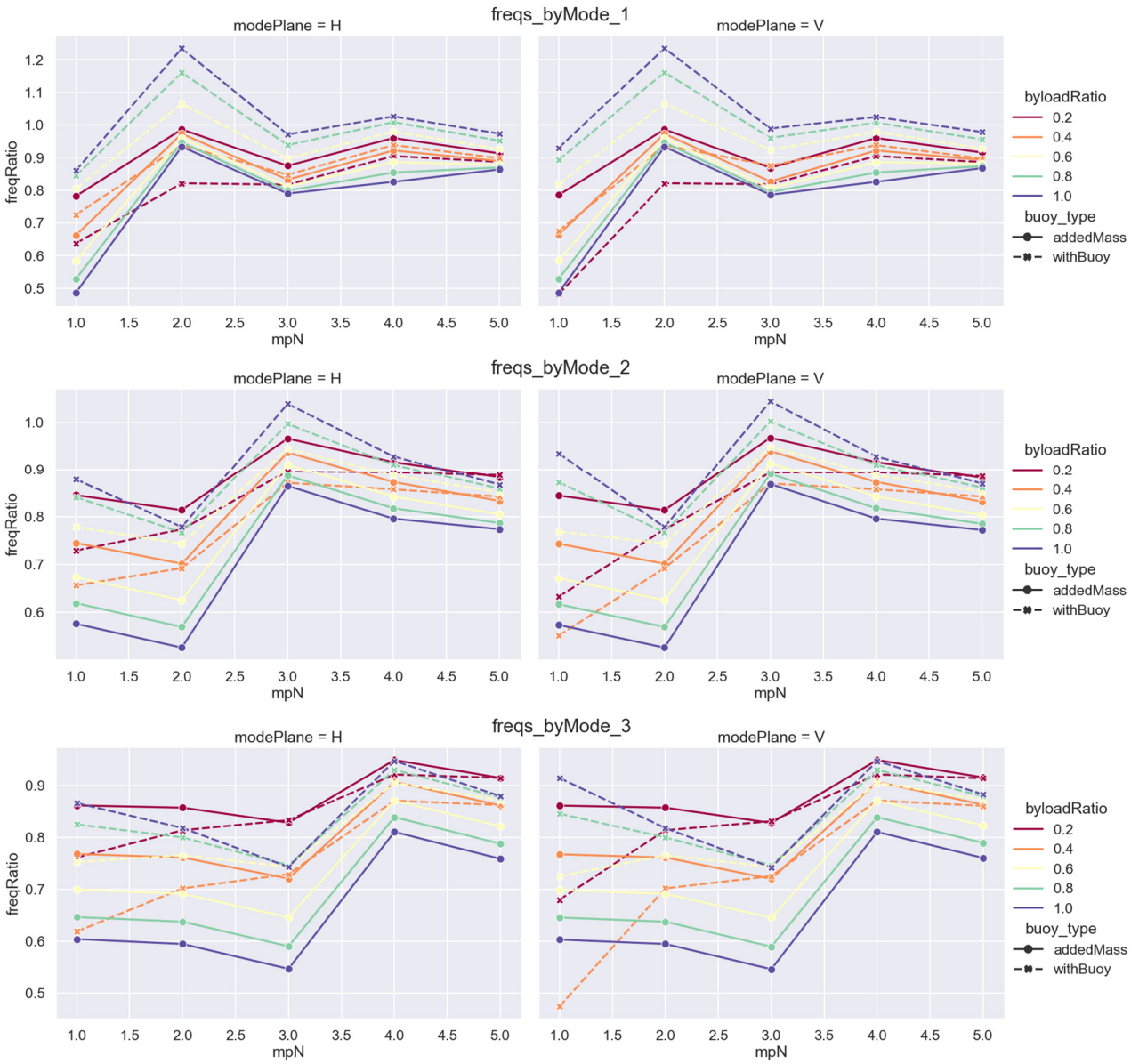


Figure 10. Comparisons of the ratio of the natural frequency of the pipelines (length = 100 m, r_p = 0.3 m, thickness = 0.02 m) against the mode numbers (mpN) for various combinations of the buoyancy modules (i.e., n = 1, 2, and 3) and load ratios (i.e., LR = 0.2, 0.4, 0.6, 0.8, and 1), where the columns are the mode plans (i.e., horizontal (**left**) and vertical (**right**)) and the rows are the number of buoyancy modules (i.e., 1, 2, and 3 buoyancy modules).

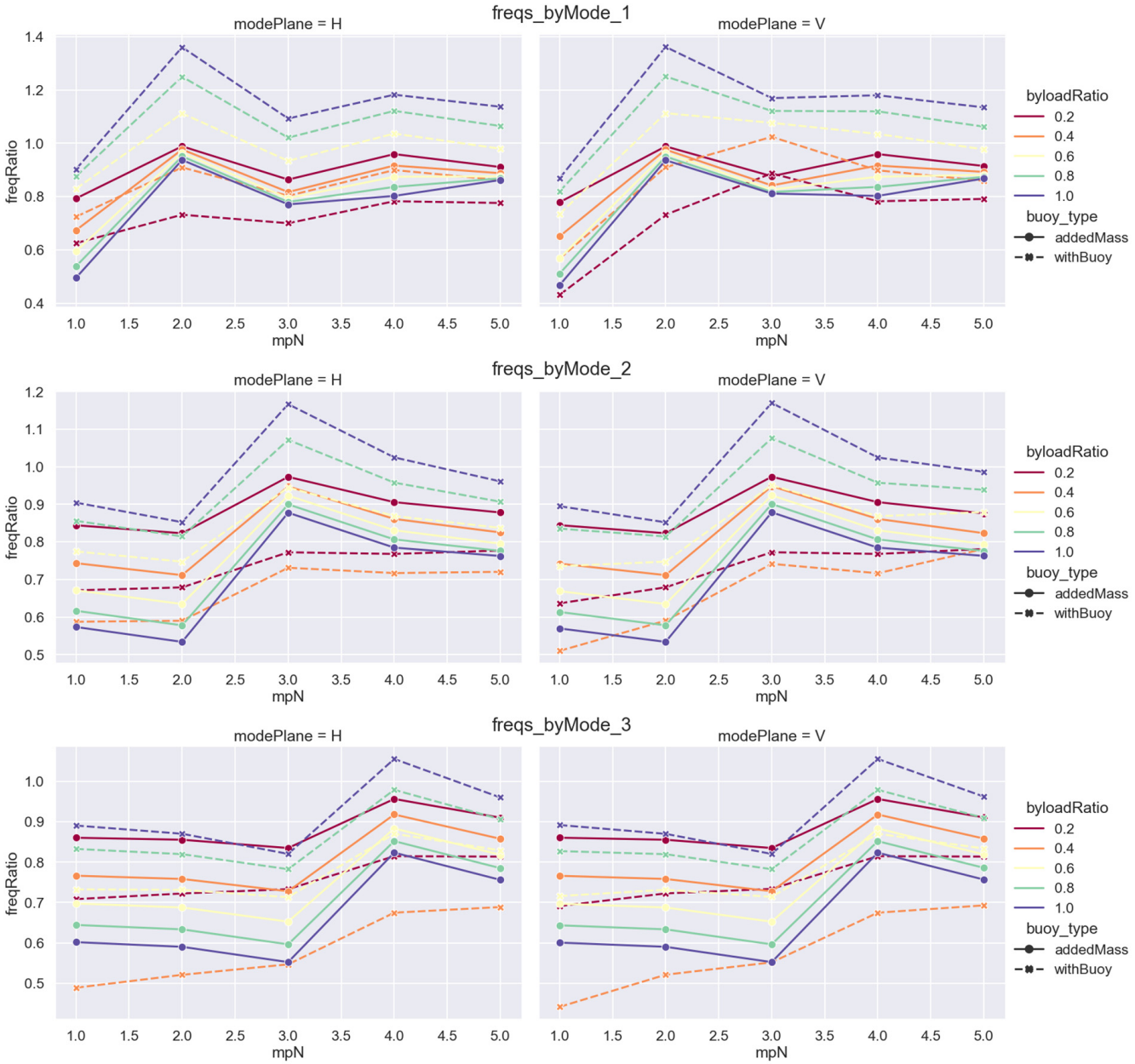


Figure 11. Comparisons of the ratio of the natural frequency of the pipelines (length = 200 m, r_p = 0.3 m, thickness = 0.02 m) against the mode numbers (mpN) for various combinations of the buoyancy modules (i.e., n = 1, 2, and 3) and load ratios (i.e., LR = 0.2, 0.4, 0.6, 0.8, and 1), where the columns are the mode plans (i.e., horizontal (**left**) and vertical (**right**)) and the rows are the number of buoyancy modules (i.e., 1, 2, and 3 buoyancy modules).

Figure 14 illustrates the same parametric analysis for fixed–fixed pipelines with identical radii of 0.30 m (a) and 0.40 m (b). Compared to the pinned–pinned configuration, the fixed–fixed support condition results in lower displacements and stresses due to its greater structural restraint. Notably, the bending moments increase more significantly with the load ratio in the fixed–fixed case; however, optimal buoyancy module placement still effectively reduces the peak moment values.

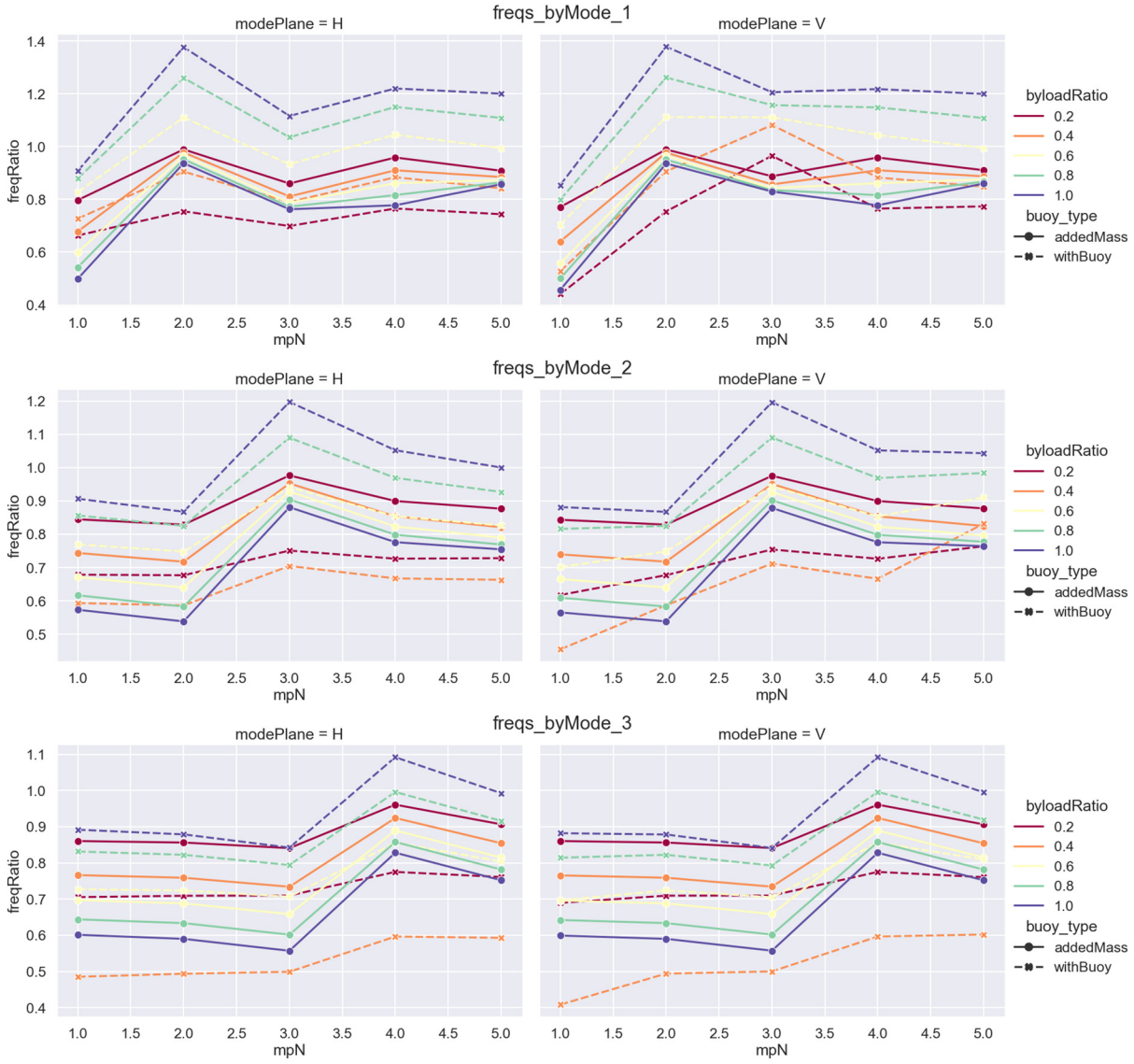


Figure 12. Comparisons of the ratio of the natural frequency of the pipelines (length = 300 m, r_p = 0.3 m, thickness = 0.02 m) against the mode numbers (mpN) for various combinations of the buoyancy modules (i.e., n = 1, 2, and 3) and load ratios (i.e., LR = 0.2, 0.4, 0.6, 0.8, and 1), where the columns are the mode plans (i.e., horizontal (**left**) and vertical (**right**)) and the rows are the number of buoyancy modules (i.e., 1, 2, and 3 buoyancy modules).

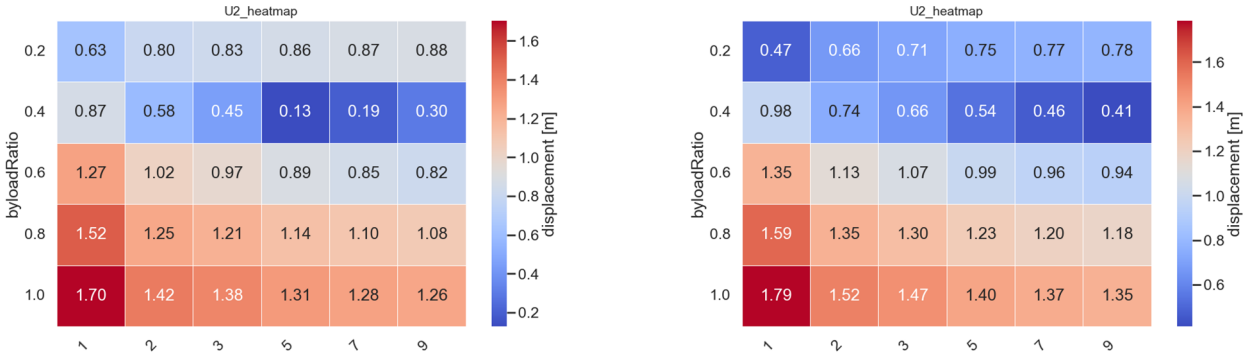
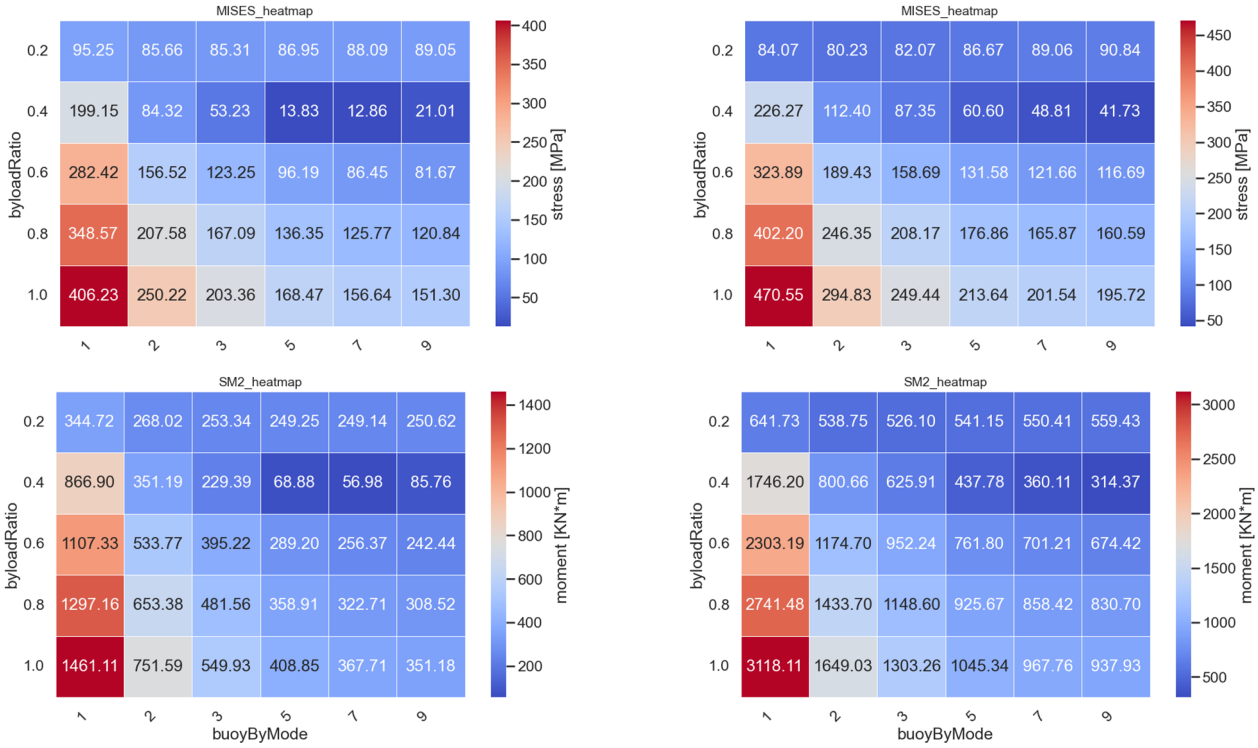


Figure 13. *Cont.*



(**a**) (**b**)

Figure 13. Heatmap results for a 100 m pinned–pinned submarine pipeline, showing displacement, von Mises stress, and bending moment for varying load ratios and buoyancy configurations: (**a**) r_p= 0.30 m; (**b**) r_p= 0.40 m.

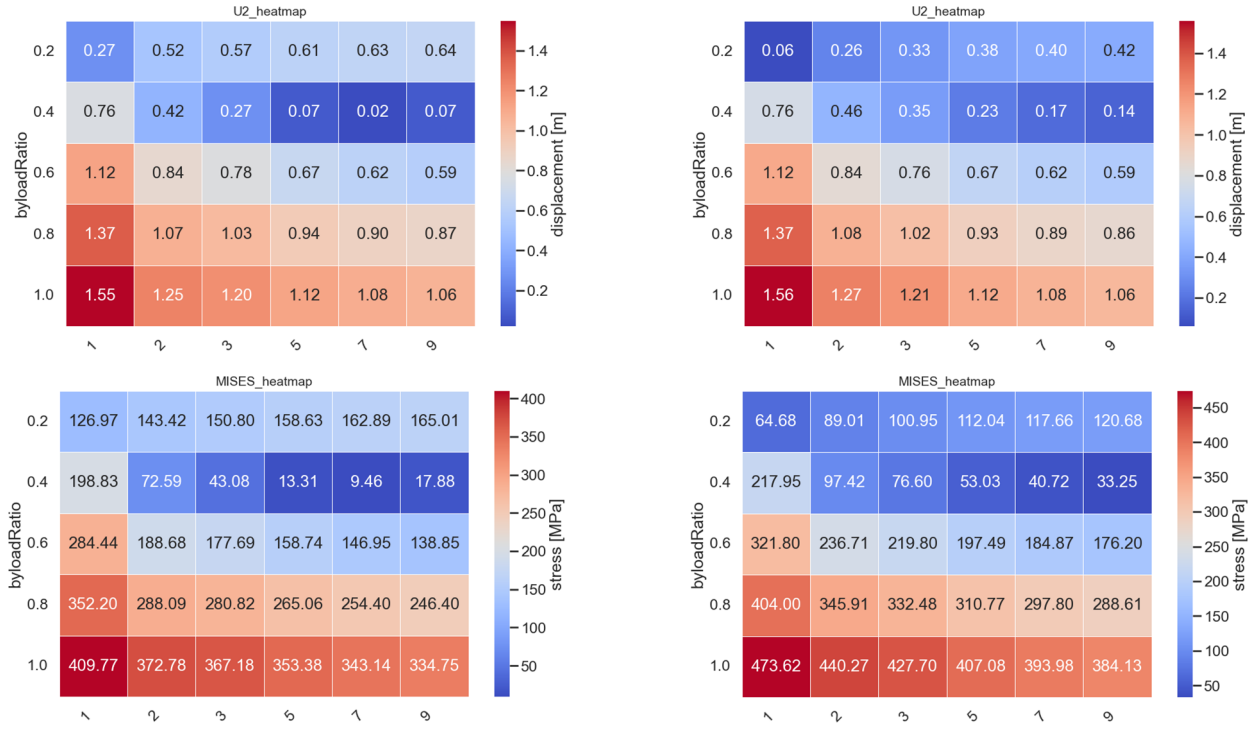
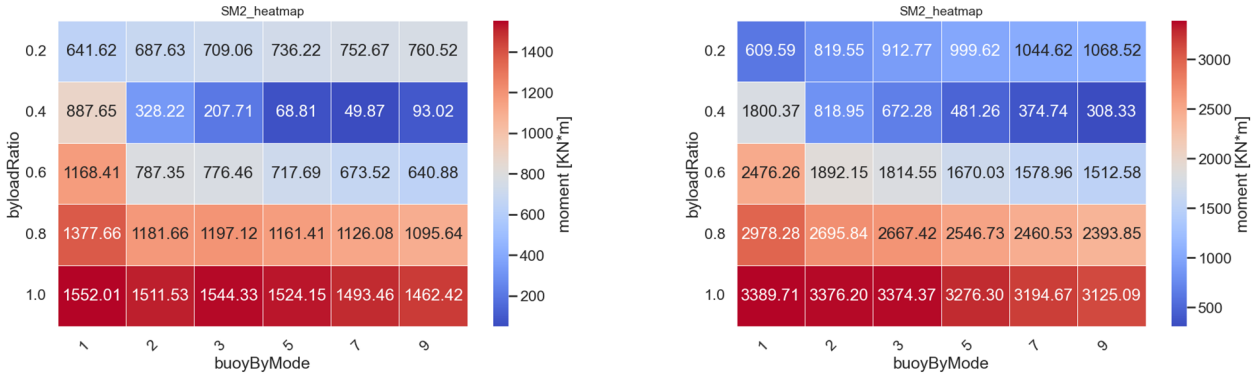


Figure 14. *Cont.*



(**a**) (**b**)

Figure 14. Heatmap results for a 100 m fixed–fixed submarine pipeline, showing displacement, von Mises stress, and bending moment for varying load ratios and buoyancy configurations: (**a**) r_p= 0.30 m; (**b**) r_p= 0.40 m.

Overall, the results underscore the importance of strategic buoyancy module placement. Configurations involving a moderate number of buoyancy modules (typically 5 to 7) offer the most efficient structural performance. Additionally, fixed–fixed boundary conditions and increased pipe radii further enhance the structural response under comparable loading conditions.

4. Discussion

This study introduces an automated Python–Abaqus computational framework developed specifically for analyzing long free-spanning submarine pipelines equipped with buoyancy modules. The results obtained through this framework demonstrate strong agreement with established analytical and numerical solutions, validating the model's reliability. Parametric analyses revealed that the pipeline's structural response, including natural frequency and static deformation, is significantly influenced by pipeline dimensions, buoyancy module arrangements, and load ratios. By indirectly representing buoyancy modules through effective density adjustments, the computational complexity is notably reduced, facilitating rapid and extensive parametric analyses. Consequently, the proposed methodology fills a critical gap in the existing literature, providing a practical and scalable tool for preliminary design, optimization of buoyancy configurations, and risk mitigation of vortex-induced vibrations (VIVs).

4.1. Mode Shape Observations

From the results, it is evident that the natural frequency and deformation of long free-spanning submarine pipelines are highly sensitive to the combination of load ratios, buoyancy modules, pipe thickness, and pipe radius. However, it can be observed that the normalized mode shape remains almost unaffected by variations in the pipeline length, radius, load ratios, buoyancy modules, and support types (i.e., fixed–fixed). This observation is clearly demonstrated in Figures 15 and 16, which compare the normalized vertical and horizontal mode shapes, respectively, of a pipeline (i.e., l_p = 300 m r_p = 0.3 m and thickness = 0.02 m) with different numbers of buoyancy modules attached ($l_b = 1/10 \cdot l_p$) (i.e., n = 0, 1, 2, 3, 5, 7, and 9), resting on fixed–fixed supports at different load ratios (i.e., *LR* = 0.2, 0.4, 0.6, 0.8, and 1). The figure shows that the mode shapes (i.e., 1, 2, 3, 4, and 5) remain consistent across the different parameters, indicating that they are not affected by variations in the system. However, it can also be observed that the mode shape of the pipeline without buoyancy modules is significantly smaller than that of the pipeline with the buoyancy modules, especially for the higher modes (i.e., 3, 4, 5).

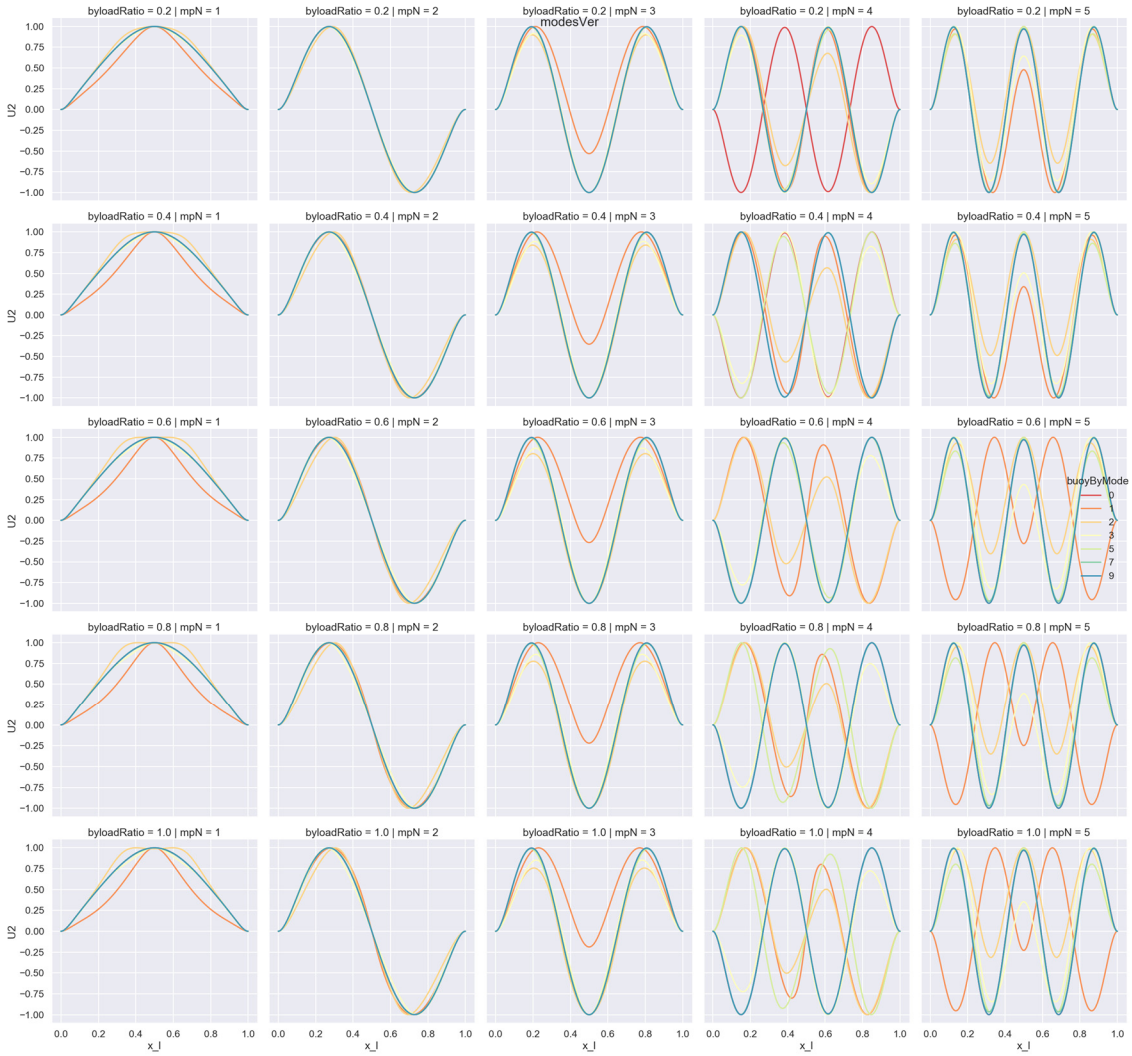


Figure 15. Comparisons of the normalized vertical mode shapes of the pipeline (i.e., $l_p = 300$ m, $r_p = 0.3$ m, and thickness = 0.02 m) with different numbers of buoyancy modules (i.e., $n = 0$, 1, 2, 3, 5, 7, and 9) resting on fixed–fixed supports, where columns are the number of mode shapes (i.e., 1, 2, 3, 4, and 5) and rows are the load ratios (i.e., LR = 0.2, 0.4, 0.6, 0.8, and 1).

4.2. Effects of Buoyancy Modules

From a Computational Fluid Dynamics (CFD) engineering standpoint, resonance poses a critical risk for submarine free-spanning pipelines, as it can induce unstable oscillatory vibrations and large amplitudes, leading to structural collapse. Specifically, the resonance phenomenon in a pipeline with buoyancy modules occurs when the vortex-induced vibration frequency—influenced by factors such as flow velocity and kinematic viscosity—aligns with the natural frequency of the pipeline–buoyancy module system computed under still-water conditions. In this regard, the present work provides valuable insights by computing the pipeline's natural frequency while accounting for different buoyancy module configurations.

Consequently, with the methodology developed in this paper, numerous scenarios for computing the deformation and frequency of the pipeline–buoyancy module system can be performed. Consequently, by tuning the buoyancy modules, the natural frequency of a long subsea pipeline with buoyancy modules may be computed and secured from the resonance at any specific mode shape. For instance, for all load ratios (i.e., 0.2, 0.4, 0.6, 0.8, and 1), the maximum frequency ratios are found at mode plan numbers (mpN) 2, 3, and 4 for 1, 2, and 3 buoyancy modules respectively. Therefore, the resonance phenomenon

of the pipeline at any specific mode can be avoided by attaching the buoyancy modules corresponding to its failure load.

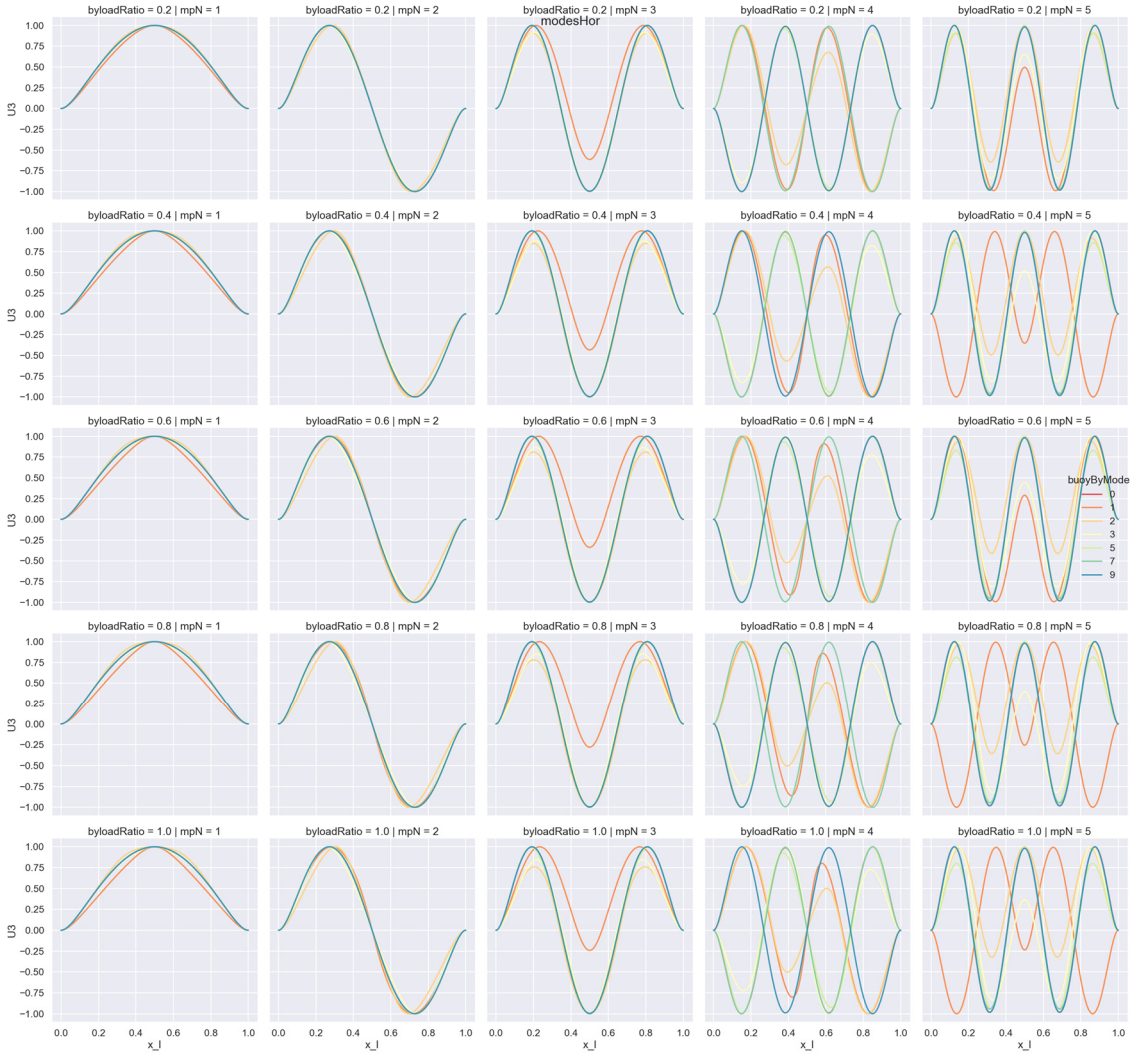


Figure 16. Comparisons of the normalized horizontal mode shapes of the pipeline (i.e., $l_p = 300$ m, $r_p = 0.3$ m, and thickness = 0.02 m) with different numbers of buoyancy modules attached (i.e., $n = 0$, 1, 2, 3, 5, 7, and 9), resting on fixed–fixed supports, where columns are the number of mode shapes (i.e., 1, 2, 3, 4, and 5) and rows are the load ratios (i.e., *LR* = 0.2, 0.4, 0.6, 0.8, and 1).

4.3. Practical Implications and Framework Advancements

The computational framework developed in this research significantly improves the efficiency of preliminary design evaluations for subsea pipelines by automating complex analyses. Engineers can rapidly investigate and compare numerous design scenarios involving varied pipeline dimensions, buoyancy module placements, and load conditions. Practically, this enables the swift identification of optimal buoyancy arrangements that can enhance pipeline stability, reduce VIV risks, and prevent resonance-induced failures. Consequently, this methodology not only streamlines computational processes but also reduces preliminary design costs and improves the safety and economic viability of offshore pipeline projects.

Moreover, this research advances existing computational approaches by replacing conventional explicit geometric modeling of buoyancy modules with an indirect method based on effective density adjustments. This innovation dramatically reduces computational complexity and processing time, enabling efficient handling of large-scale parametric

analyses. Such automation alleviates the burdens associated with traditional FEA modeling, making extensive scenario analysis practical. The demonstrated accuracy and reliability of this simplified approach highlight its suitability for engineering applications, offering a robust and streamlined method for the preliminary design and optimization of subsea pipelines with buoyancy modules.

4.4. Limitations and Future Research

Despite demonstrating high reliability and accuracy, the current computational framework presents certain limitations. It assumes linear elastic material behavior and excludes nonlinear phenomena such as large deformations, material plasticity, and detailed fluid–structure interactions. Additionally, environmental factors such as seabed irregularities, current dynamics, and temperature variations were not explicitly modeled.

The present study emphasizes static and modal analyses to validate the proposed computational framework. However, dynamic responses, such as vortex-induced vibrations (VIVs) under oscillatory waves and current loading, as well as environmental influences like seabed currents, can significantly affect pipeline behavior. Recent work by Zhu et al. (2024) underscores the importance of accounting for seabed heterogeneity and liquefaction potential in wave-induced response analyses around buried pipelines [39]. In addition, studies by Weng et al. (2023) and Xu et al. (2025) demonstrate that incorporating fluid–structure interaction models can substantially modify predictions of pipeline fatigue life and structural integrity under complex loading scenarios [40,41]. These advanced modeling approaches represent valuable extensions to the simplified framework proposed here. While our method provides an efficient tool for preliminary design and parametric assessment, practitioners should be aware that neglecting such interactions may result in conservative or non-conservative estimations, particularly in dynamic offshore environments with variable seabed properties.

Validation of the proposed computational framework is essential to ensure its accuracy and reliability. However, conducting full-scale experimental validation was not feasible in this study due to the high costs associated with fabricating and deploying long-span (100–300 m) pipelines, as well as logistical complexities, administrative coordination with regulatory authorities, prohibitive operational expenses, and limited site access. Additionally, collaboration with industry partners was not achievable. Given these constraints, the validation was performed through comparisons with established analytical solutions and numerical benchmarks from references such as DNVGL-RP-F105 [17], Palmer and King [1], and Phuor et al. [16]. The strong agreement between the computational results and these benchmarks confirms the reliability and validity of the proposed computational framework. However, to fully validate and generalize the findings presented here, future studies involving full-scale experimental validation or carefully designed scaled physical modeling are recommended.

Future research should aim to address these limitations by incorporating nonlinear dynamic effects and more advanced fluid–structure interaction analyses. Furthermore, integrating realistic seabed conditions and complex environmental factors into the framework will enhance its practical applicability and accuracy. Advanced optimization methods, such as genetic algorithms or machine learning techniques, could also be explored to further optimize buoyancy module configurations. These advancements would provide engineers and researchers with more comprehensive tools, facilitating safer and economically optimized designs for subsea pipelines operating in challenging marine environments.

In addition, emerging artificial intelligence (AI) and machine learning (ML) techniques hold great potential for enhancing predictive accuracy and computational efficiency in subsea pipeline analysis, as already demonstrated in various engineering domains [42–45].

Furthermore, several studies have shown that ML algorithms can successfully predict vortex-induced vibrations (VIVs) and related dynamic responses in a range of structural and offshore engineering contexts [46,47]. These technologies can support the identification of optimal buoyancy module arrangements, uncover complex nonlinear patterns in large simulation datasets, and enable real-time structural health monitoring under variable environmental conditions. Integrating AI and ML into the current framework may lead to adaptive, data-driven models that are capable of continuously improving design strategies and mitigating risk in dynamic marine environments.

5. Conclusions

This study presents an advanced Python–Abaqus integrated computational framework developed for analyzing the structural behavior of long free-spanning submarine pipelines under various buoyancy module configurations. The framework effectively addresses key challenges inherent in traditional finite element modeling, including extensive computational effort and cumbersome manual data handling, by employing automated data processing and indirect modeling through effective density adjustments.

A comprehensive set of 1260 model simulations were conducted to investigate the behavior of free-span undersea pipelines. The simulations covered various combinations of pipeline lengths (100, 200, and 300 m), radii (0.3, 0.4, and 0.5 m), pipe thicknesses (0.02 and 0.03 m), buoyancy module configurations (n = 0, 1, 2, 3, 5, 7, and 9), and load ratios (ranging from 0 to 1). The accuracy and robustness of the proposed framework were validated against established analytical and numerical solutions, with strong agreement observed across different scenarios.

The results highlighted that there is a clear relationship between pipeline length, radius, and the resulting frequency and deformation characteristics. It was observed that the frequency decreases as the pipeline length increases. However, as the pipeline length increases, the deformation also increases. Additionally, when considering the radius of the pipe, it was observed that the deformation decreases as the radius increases.

Furthermore, the behavior of pipelines with buoyancy modules ($n > 0$) exhibits significant dependence on the load ratio (LR), the number of buoyancy modules (n), and the pipe radius and thickness, affecting both the natural frequency and deformation characteristics. Consequently, it is unnecessary to attach numerous buoyancy modules uniformly along the pipeline to minimize deformation and natural frequency. Additionally, discussions on the mode shapes of free-spanning pipelines, with and without buoyancy modules, reveal minimal changes in the normalized mode shapes due to the attachment of buoyancy modules. These mode shapes exhibit negligible sensitivity to variations in pipeline length and radius, load ratio, and buoyancy module placement on the fixed–fixed support.

The findings offer valuable insights into the analysis of long free-span pipelines in conjunction with buoyancy modules. These results provide a potential solution for mitigating the resonant vortex-induced vibration (VIV) in lengthy underwater pipelines by utilizing buoyancy modules. For instance, the maximum frequency ratios were found for the mode plan numbers (mpN) 2, 3, and 4 for 1, 2, and 3 buoyancy modules, respectively, for all load ratios. Therefore, the frequency magnitude at a specific mode might be changed with the installation of the buoyancy module. Consequently, by understanding the effects of buoyancy modules on the natural frequency and deformation characteristics, engineers and researchers can gain valuable knowledge for designing long free-span pipelines and optimizing their performance. Additionally, it should be noted that the framework developed in this paper may also be capable of predicting the behavior of free multi-span pipelines.

This study provides a valuable computational tool and insights into submarine pipelines' stability, aiding engineers in designing and optimizing pipeline–buoyancy mod-

ule configurations to avoid resonance-induced structural failures. Future research is encouraged to incorporate nonlinear dynamic effects, advanced fluid–structure interaction analyses, and further optimization techniques to expand the practical applicability and effectiveness of the developed methodology in realistic offshore conditions.

Supplementary Materials: The following supporting information can be downloaded at https://www.mdpi.com/article/10.3390/math13091387/s1: Figure S1. Comparisons of the vertical deformation of the pipelines ($r_p = 0.4$ m and thickness $(t_p) = 0.02$ m) with various numbers of buoyancy modules attached ($l_b = 1/10 \cdot l_p$), with different load ratios (i.e., *LR* = 0.2, 0.4, 0.6, 0.8, and 1, with different colors), against the pipe length resting on the fixed–fixed support, where columns are the pipe length (i.e., 100, 200, 300 m) and rows are the number of buoyancy modules ($l_b = 1/10 \cdot l_p$) (i.e., n (=buoyByMode) = 0, 1, 2, 3, 5, 7, and 9). Figure S2. Comparisons of the vertical deformation of the pipelines ($r_p = 0.5$ m and thickness $(t_p) = 0.03$ m) with various numbers of buoyancy modules attached ($l_b = 1/10 \cdot l_p$), with different load ratios (i.e., *LR* = 0.2, 0.4, 0.6, 0.8, and 1, with different colors), against the pipe length resting on the fixed–fixed support, where columns are the pipe length (i.e., 100, 200, 300 m) and rows are the number of buoyancy modules ($l_b = 1/10 \cdot l_p$) (i.e., n (=buoyByMode) = 0, 1, 2, 3, 5, 7, and 9). Figure S3. Comparisons of the ratio of the natural frequency of the pipelines (length = 300 m, $r_p = 0.3$ m, thickness = 0.03 m) against the mode numbers (mpN) for various combinations of the buoyancy modules (i.e., $n = 1$, 2, and 3) and load ratios (i.e., *LR* = 0.2, 0.4, 0.6, 0.8, and 1), where columns are the mode plans (i.e., horizontal (left) and vertical (right)) and rows are the number of buoyancy modules (i.e., 1, 2, and 3 buoyancy modules). Figure S4. Comparisons of the ratio of the natural frequency of the pipelines (length = 300 m, $r_p = 0.5$ m, thickness = 0.03 m) against the mode numbers (mpN) for various combinations of the buoyancy modules (i.e., $n = 1$, 2, and 3) and load ratios (i.e., *LR* = 0.2, 0.4, 0.6, 0.8, and 1), where columns are the mode plans (i.e., horizontal (left) and vertical (right)) and rows are the number of buoyancy modules (i.e., 1, 2, and 3 buoyancy modules).

Author Contributions: Writing—original draft preparation, T.P.; writing—review and editing, T.P., A.G., A.U. and P.A.T.; visualization, T.P., A.G., A.U. and P.A.T.; supervision, A.G. and P.A.T.; project administration, A.G. and P.A.T.; funding acquisition, A.G. and P.A.T. All authors have read and agreed to the published version of the manuscript.

Funding: This research was funded by Israel's Ministry of Energy, grant number 220-17-007.

Data Availability Statement: The datasets generated and/or analyzed in the present study are available from the corresponding author upon reasonable request.

Acknowledgments: The support from Israel's Ministry of Energy [grant number 220-17-007] is gratefully acknowledged.

Conflicts of Interest: The authors declare no conflict of interest.

Abbreviations

A_{fpc}	Cross-sectional area of the fluid, pipe, and coating
A_{bNp}	Cross-sectional area of the buoyancy module, and the density of seawater
Def	Vertical deformation of the pipeline
FEA	Finite element analysis
g	Gravitational acceleration
l_b	Length of a single buoyancy module
l_p	Length of the pipeline
L/D	Length-to-diameter ratio
LR	Load ratio
m_p	Mass of the steel pipe
m_c	Mass of the coating
m_f	Mass of the fluid (oil, gas, etc.)

$m_{w,fpc}$	Mass of pushed water displaced by the fluid, pipe, and concrete
$m_{w,b}$	Mass of pushed water displaced by the fluid, pipe, concrete, and buoyancy module
n	Number of buoyancy modules
PS	Present solution (developed Python–Abaqus framework)
r_p	Outer radius of the pipeline
ρ_w	Density of seawater
t_p	Pipe wall thickness
VIV	Vortex-induced vibration

Appendix A



Figure A1. *Cont.*

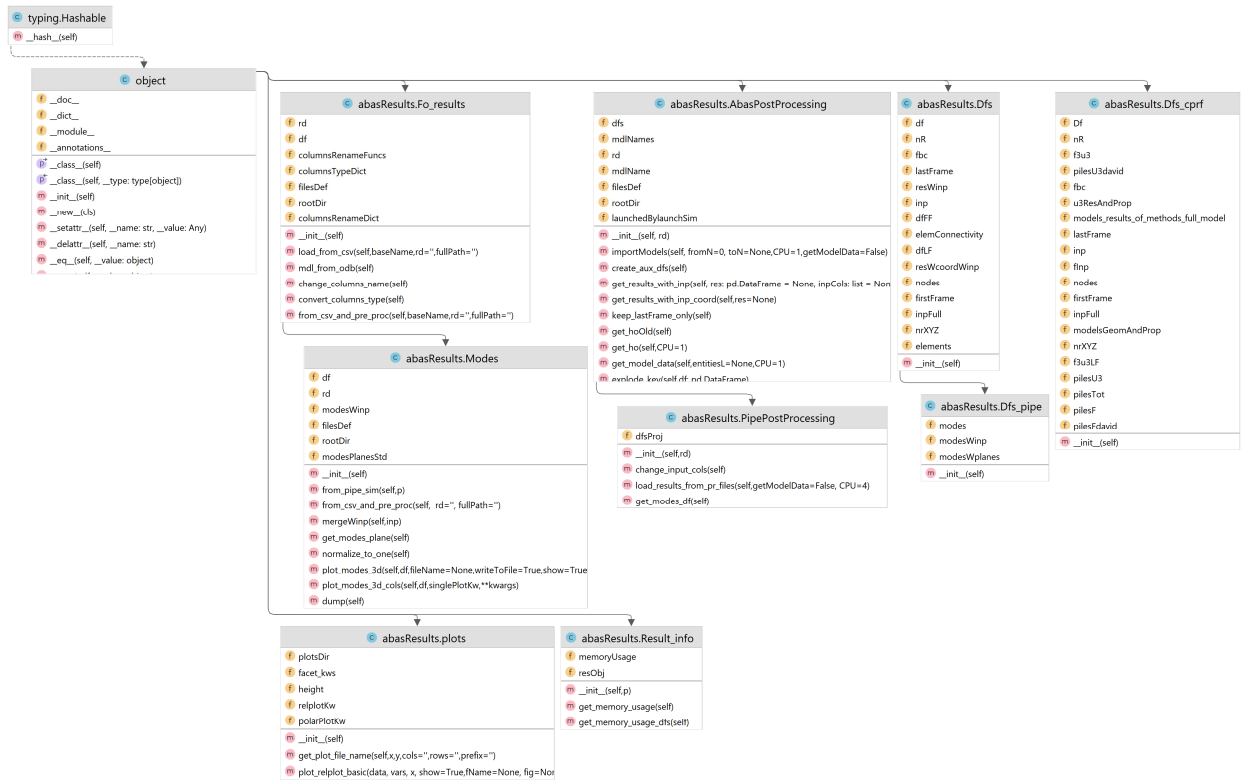


Figure A1. Python-Abaqus classes and methods diagram.

References

1. Palmer, A.; King, R. *Subsea Pipeline Engineering—Google Books*; Pennwell Publishing: Tulsa, OK, USA, 2004.
2. Elosta, H.; Huang, S.; Incecik, A. Wave Loading Fatigue Reliability and Uncertainty Analyses for Geotechnical Pipeline Models. *Ships Offshore Struct.* **2014**, *9*, 450–463. [CrossRef]
3. Trapper, P.A.; Mishal, I. Numerical Analysis of Offshore Pipe-Lay Subjected to Environment-Induced Non-Uniformly Distributed Follower Loads. *Appl. Ocean Res.* **2020**, *100*, 102149. [CrossRef]
4. Banić, D.; Turkalj, G.; Kvaternik Simonetti, S.; Lanc, D. Numerical Model for a Geometrically Nonlinear Analysis of Beams with Composite Cross-Sections. *J. Compos. Sci.* **2022**, *6*, 377. [CrossRef]
5. Xiao, Z.; Zhao, X. Prediction of Natural Frequency of Free Spanning Subsea Pipelines. *Int. J. Steel Struct.* **2010**, *10*, 81–89. [CrossRef]
6. Bai, Q.; Bai, Y. *Subsea Pipeline Design, Analysis, and Installation*; Elsevier: Amsterdam, The Netherlands, 2014.
7. Kim, D.K.; Incecik, A.; Choi, H.S.; Wong, E.W.C.; Yu, S.Y.; Park, K.S. A Simplified Method to Predict Fatigue Damage of Offshore Riser Subjected to Vortex-Induced Vibration by Adopting Current Index Concept. *Ocean Eng.* **2018**, *157*, 401–411. [CrossRef]
8. Liu, G.; Li, H.; Xie, Y.; Incecik, A.; Li, Z. Investigating Cross-Flow Vortex-Induced Vibration of Top Tension Risers with Different Aspect Ratios. *Ocean Eng.* **2021**, *221*, 108497. [CrossRef]
9. Song, Q.; Liu, J.; Gao, F. Very High Cycle Fatigue Life of Free-Spanning Subsea Pipeline Subjected to Vortex-Induced Vibrations. *J. Mar. Sci. Eng.* **2024**, *12*, 1556. [CrossRef]
10. Lu, Y.; Liu, Z.; Xu, W.; Ma, Y. Vortex-Induced Vibration (VIV) Fatigue Damage Characteristics of Submarine Multispan Pipelines. *Ocean Eng.* **2025**, *324*, 120666. [CrossRef]
11. Zou, X.; Xie, B.; Zang, Z.; Chen, E.; Hou, J. Vortex-Induced Vibration and Fatigue Damage Assessment for a Submarine Pipeline on a Sand Wave Seabed. *J. Mar. Sci. Eng.* **2023**, *11*, 2031. [CrossRef]
12. Elosta, H.; Huang, S.; Incecik, A. Seabed Interaction Modeling Effects on the Global Response of Catenary Pipeline: A Case Study. *J. Offshore Mech. Arct. Eng.* **2014**, *136*, 032001. [CrossRef]
13. Sun, J.; Huang, S. Pipeline Spanning. In *Encyclopedia of Maritime and Offshore Engineering*; Wiley: Hoboken, NJ, USA, 2017; pp. 1–9.
14. Trapper, P.A. Static Analysis of Offshore Pipe-Lay on Flat Inelastic Seabed. *Ocean Eng.* **2020**, *213*, 107673. [CrossRef]
15. Wang, F.C.; Han, L.H. Analytical Behavior of Carbon Steel-Concrete-Stainless Steel Double-Skin Tube (DST) Used in Submarine Pipeline Structure. *Mar. Struct.* **2019**, *63*, 99–116. [CrossRef]
16. Phuor, T.; Trapper, P.A.; Ganz, A. An Analytical Expression for the Fundamental Frequency of a Long Free-Spanning Submarine Pipeline. *Mathematics* **2023**, *11*, 4481. [CrossRef]

17. DNVGL. *DNVGL-RP-F105: Free Spanning Pipelines*; DNV GL: Belum, Norway, 2017.
18. Gvirtzman, Z.; Reshef, M.; Buch-Leviatan, O.; Groves-Gidney, G.; Karcz, Z.; Makovsky, Y.; Ben-Avraham, Z. Bathymetry of the Levant Basin: Interaction of Salt-Tectonics and Surficial Mass Movements. *Mar. Geol.* **2015**, *360*, 25–39. [CrossRef]
19. Sarpkaya, T. A Critical Review of the Intrinsic Nature of Vortex-Induced Vibrations. *J. Fluids Struct.* **2004**, *19*, 389–447. [CrossRef]
20. Beckmann, M.M.; Hale, J.R.; Lamison, C.W. Spanning Can Be Prevented, Corrected in Deeper Water. *Oil Gas J.* **1991**, *89*, 84–89.
21. Choi, H.S. Free Spanning Analysis of Offshore Pipelines. *Ocean Eng.* **2001**, *28*, 1325–1338. [CrossRef]
22. Vedeld, K.; Sollund, H.; Hellesland, J. Free Vibrations of Free Spanning Offshore Pipelines. *Eng. Struct.* **2013**, *56*, 68–82. [CrossRef]
23. Gullaksen, J. Implementation of a Method for Free-Spanning Pipeline Analysis. In *International Conference on Offshore Mechanics and Arctic Engineering—OMAE*; American Society of Mechanical Engineers: New York, NY, USA, 2021; Volume 4.
24. Bao, R.D.; Wen, B.C. Dynamic Response Analysis of Submarine Free Spanning Pipeline. *Zhendong Yu Chongji/J. Vib. Shock* **2007**, *26*, 140–143.
25. Rumson, A.G. The Application of Fully Unmanned Robotic Systems for Inspection of Subsea Pipelines. *Ocean Eng.* **2021**, *235*, 109214. [CrossRef]
26. Yaghoobi, M.; Mazaheri, S.; Jabbari, E. Determining Natural Frequency of Free Spanning Offshore Pipelines by Considering the Seabed Soil Characteristics. *J. Persian Gulf* **2012**, *3*, 25–34.
27. Sarkar, G.; Roy, P. Effect of Non-Homogeneity of Seabed Soil on Natural Frequency of Offshore Free Spanning Pipeline. In *Earthquakes and Structures*; Lecture Notes in Civil Engineering; Springer: Singapore, 2022; Volume 188.
28. Sarkar, G.; Roy, P. Influence of Seabed Soil Characteristics on Eigenfrequency of Offshore Free Spanning Pipeline. In *Advances in Offshore Geotechnics*; Lecture Notes in Civil Engineering; Springer: Singapore, 2020; Volume 92.
29. Energean. *Karish and Tanin Field Development Plan*; Energean: London, UK, 2017.
30. Schweiger, H.F.; Fabris, C.; Ausweger, G.; Hauser, L. Examples of Successful Numerical Modelling of Complex Geotechnical Problems. *Innov. Infrastruct. Solut.* **2019**, *4*, 2. [CrossRef]
31. Phuor, T.; Yoon, G.H. Eigensensitivity of Damped System with Distinct and Repeated Eigenvalues by Chain Rule. *Int. J. Numer. Methods Eng.* **2023**, *124*, 4687–4717. [CrossRef]
32. Mohaddes Pour, M.; Razavi Taheri, S.S.; Moniri Abyaneh, A. Free Span Analysis for Submarine Pipelines. *Shock Vib.* **2021**, *2021*, 9305129. [CrossRef]
33. Zhang, Z. Application of Finite Element Analysis in Structural Analysis and Computer Simulation. *Appl. Math. Nonlinear Sci.* **2024**, *9*, 9. [CrossRef]
34. Gong, S.; Xu, P.; Bao, S.; Zhong, W.; He, N.; Yan, H. Numerical Modelling on Dynamic Behaviour of Deepwater S-Lay Pipeline. *Ocean Eng.* **2014**, *88*, 393–408. [CrossRef]
35. Jiwa, M.Z.; Kim, D.K.; Mustaffa, Z.; Choi, H.S. A Systematic Approach to Pipe-in-Pipe Installation Analysis. *Ocean Eng.* **2017**, *142*, 478–490. [CrossRef]
36. Guo, B.; Song, S.; Ghalambor, A.; Lin, T. *Offshore Pipelines: Design, Installation, and Maintenance: Second Edition*; Gulf Professional Publishing: Houston, TX, USA, 2013.
37. ABAQUS. *Abaqus User's Manual Version 2022*; Dassault Systèmes Simulia Corp.: Providence, RI, USA, 2022.
38. ABAQUS. *Abaqus Version 2021-1 Analysis User's Manual*; Abaqus Online Documents 2021; Dassault Systèmes Simulia Corp.: Providence, RI, USA, 2021.
39. Zhu, B.; Yang, Q.; Wang, T.; Lu, M.; Mo, P.; Hiraishi, T.; Mase, H. Investigation on Wave-Induced Responses of Heterogeneous Seabed around a Buried Pipeline Based on Nonstationary Random Field Model. *Comput. Geotech.* **2024**, *167*, 106119. [CrossRef]
40. Weng, G.; Xu, C.; Xie, Q.; Wu, X.; Lan, G.; Zhang, Y.; Zhu, X. Dynamic Effect of Fluid–Structure Interaction and Modal Analysis of Crude–Pipeline Interaction System Considering the Fluctuating Pressure of Medium. *Transp. Res. Rec.* **2024**, *2678*, 168–188. [CrossRef]
41. Xu, H.; Guo, Q.; Wang, X.; Sun, H.; Dong, Z.; Gu, J.; Zhang, C. Dynamic Analysis of Submarine-Buried Pipelines Considering Fluid–Structure Interaction. *Water* **2025**, *17*, 360. [CrossRef]
42. Mitelman, A.; Lifshitz Sherzer, G. Coupling Numerical Modeling and Machine-Learning for Back Analysis of Cantilever Retaining Wall Failure. *Comput. Concr.* **2023**, *31*, 307–314. [CrossRef]
43. Mitelman, A.; Urlainis, A. Investigation of Transfer Learning for Tunnel Support Design. *Mathematics* **2023**, *11*, 1623. [CrossRef]
44. Eilat, T.; McQuillan, A.; Mitelman, A. Machine Learning-Enhanced Analysis of Small-Strain Hardening Soil Model Parameters for Shallow Tunnels in Weak Soil. *Geotechnics* **2025**, *5*, 26. [CrossRef]
45. Pajaziti, E.; Montalt-Tordera, J.; Capelli, C.; Sivera, R.; Sauvage, E.; Quail, M.; Schievano, S.; Muthurangu, V. Shape-Driven Deep Neural Networks for Fast Acquisition of Aortic 3D Pressure and Velocity Flow Fields. *PLoS Comput. Biol.* **2023**, *19*, e1011055. [CrossRef]

46. Wang, Z.; Zhu, J.; Zhang, Z. Machine Learning-Based Deep Data Mining and Prediction of Vortex-Induced Vibration of Circular Cylinders. *Ocean Eng.* **2023**, *285*, 115313. [CrossRef]
47. Ma, L.; Lin, K.; Fan, D.; Wang, J.; Triantafyllou, M.S. Flexible Cylinder Flow-Induced Vibration. *Phys. Fluids* **2022**, *34*, 011302. [CrossRef]

Disclaimer/Publisher's Note: The statements, opinions and data contained in all publications are solely those of the individual author(s) and contributor(s) and not of MDPI and/or the editor(s). MDPI and/or the editor(s) disclaim responsibility for any injury to people or property resulting from any ideas, methods, instructions or products referred to in the content.